#### REVIEW ARTICLE

WILEY

# Covalent organic frameworks: Design and applications in electrochemical energy storage devices

Shikai Jin<sup>1</sup> | Omar Allam<sup>1,2</sup> | Seung Soon Jang<sup>2</sup> | Seung Woo Lee<sup>1</sup> •

<sup>1</sup>George W. Woodruff School of Mechanical Engineering, Georgia Institute of Technology, Atlanta, Georgia, USA <sup>2</sup>Computational NanoBio Technology Laboratory, School of Material Science and Engineering, Georgia Institute of

Technology, Atlanta, Georgia, USA

#### Correspondence

Seung Soon Jang, Computational NanoBio Technology Laboratory, School of Material Science and Engineering, Georgia Institute of Technology, Atlanta, GA 30332, USA.

Email: seungsoon@mse.gatech.edu

Seung Woo Lee, George W. Woodruff School of Mechanical Engineering, Georgia Institute of Technology, Atlanta, GA 30332, USA.

Email: seung.lee@me.gatech.edu

#### Funding information

Division of Chemical, Bioengineering, Environmental, and Transport Systems, National Science Foundation, Grant/ Award Number: 1805052

#### Abstract

As an emerging class of crystalline organic material, covalent organic frameworks (COFs) possess uniform porosity, versatile functionality, and precise control over designated structures. Aside from the favorable charge and mass transport pathways offered by the porous framework, COFs can also exhibit designed reversible redox activity. In the past few years, their potential has attracted a great deal of attention for charge storage and transport applications in various electrochemical energy storage devices, and numerous design strategies have been proposed to enhance the corresponding electrochemical properties. This review summarizes the working principle and synthesis methods of COFs and discusses significant findings for supercapacitors and various rechargeable battery systems, emphasizing the representative design strategies and their underlying relationship with electrochemical performances. In addition, key advances achieved by computations are highlighted along with the challenges and prospects in this field.

#### KEYWORDS

covalent organic frameworks, rechargeable batteries, redox-active electrodes, solid electrolyte, supercapacitors

#### 1 | INTRODUCTION

Due to the steady increase in energy demand, the depletion of fossil fuels, and the detrimental impact of greenhouse gas emissions on the environment, finding alternative renewable energy resources as well as developing high-capacity energy storage technologies have been major challenges for modern civilization. At the same time, rapid advancements in consumer electronics and electric vehicles have also entailed increasing demands for safe and efficient energy storage solutions. In this context, a general consensus is that developing electrochemical energy storage (EES) devices is the most promising

solution for such growing demands, which is mainly due to their promising high performance with relatively low cost and excellent stability. Therefore, a great deal of research effort has been devoted to the development of EES systems, such as supercapacitors and various types of batteries, which are safe, inexpensive, and environmentally friendly. Lithium-ion batteries (LIBs) exhibit the highest energy density among EES systems. However, LIBs employ inorganic electrode materials such as transition-metal oxides, which often exhibit limited capacity and are of high scarcity. Recently, organic electrode materials have risen due to numerous advantages over their inorganic counterpart.<sup>2–5</sup> First, organic electrode

This is an open access article under the terms of the Creative Commons Attribution License, which permits use, distribution and reproduction in any medium, provided the original work is properly cited.

© 2022 The Authors. *InfoMat* published by UESTC and John Wiley & Sons Australia, Ltd.

InfoMat. 2022;1–35. wileyonlinelibrary.com/journal/infomat

materials consisting of abundant elements (e.g., C, H, O, N, and S) can be obtained through environmentally friendly synthesis processes.<sup>5,6</sup> Moreover, organic electrode materials bearing redox-active functional groups are often capable of higher capacities, and their structures are also flexible and can be easily tuned to meet specific engineering requirements. Last, organic electrode materials can be integrated with various charge storage mediums, which allows one type of organic electrode to be utilized in various EES systems with different counterions.

Among various organic materials for EES systems, covalent organic frameworks (COFs) have attracted lots of attention in recent years. COF is an emerging class of porous, crystalline polymer formed by covalent bonds among molecular components, 7,8 which has several favorable traits such as long-range order, high and uniform porosity, a stable functional skeleton in addition to a high degree of freedom for structural design and property manipulation. These characteristics make COFs applicable to a wide range of applications, including gas storage and separation, 9-13 catalysis, 14-16 sensing, 17-20 optoelectronics, <sup>21–26</sup> drug delivery, <sup>27–29</sup> as well as energy conversion and storage. 30-32 In particular, COF is considered a promising candidate for various components in EES systems owing to its unique features. The uniformly porous structure yields a high surface area and enables precise structural design to optimize its mass and charge transport properties. The freedom to incorporate functional components within the stable framework also allows the integration of redox-active moieties for reversible redox processes, while preventing them from dissolution and degradation in the aprotic electrolytes. Therefore, COFs have been utilized as active organic electrode materials as well as electrolytes and separators in various EES systems. 32-34 Although not covered in this review, it is also worth noting that highly efficient COF electrocatalysts are also employed for energy conversion in metal-air batteries<sup>35–38</sup> and fuel cells.<sup>39,40</sup>

Since its first introduction in 2005, the exploration of COF materials and their utilization in EES systems is still in its infancy. Current studies of COFs are mostly focused on 2D binary functional design and postprocesses for structural modifications. 31,41,42 Research efforts devoted toward various EES systems, though at different stages of development, often reveal recurring concepts and design principles applicable for other electrochemical processes as well. While COFs had been introduced in several comprehensive reviews 8,34,43-45 as well as ones regarding specific EES systems, 31,32,41,46 few discussions were made to present the fundamental understanding of the working principles and design strategies of COFs in order to improve electrochemical performance for EES. In this review, we will introduce the formation mechanism and

synthesis methods of COF, and then present significant findings in EES applications through emphasizing the representative design approaches (Figure 1) utilized in each field and their underlying relationships with electrochemical performances. Given the significance of computational methods for COF in structural design and prediction of properties, important findings made by modeling and simulation will also be covered. Lastly, we will offer some perspective regarding the challenges and opportunities for further research in this field.

# 2 | WORKING PRINCIPLE AND CHARGE STORAGE MECHANISM OF COF

### 2.1 | Covalent bond formation and structure

Covalent bonding has traditionally been utilized successfully to synthesize small organic molecules with the desired structure and functionality. However, such methods could not be applied to supramolecular schemes to design any lattice structure with long-range order. Because the orientation of bonding cannot be precisely controlled during the growth period, the polymers formed by means of covalent bonding are mostly amorphous, especially in higher dimensions (2D/3D).8 This is a major obstacle to the design and engineering of organic materials as its amorphous structure interferes with accurate crystallographic measurements and control of structures and properties on the atomic scale. The crystal structure of COFs is achieved by utilizing microscopic reversible reactions that form covalent bonds, while allowing thermodynamically driven error-correction during crystal growth. 44,47 Of all possible bonds and orientations, the establishment of a stable, uniform, and long-range supramolecular structure depends on the elimination of energetically unstable configuration and the growth of equilibrium structure by reverse bonding reactions. Intricate synthetic conditions and processes are required to maintain the reversibility of the reaction. The geometry of COF structure depends on the combination of symmetries exhibited by each building block and their orientations in the framework. Therefore, the participating moieties must be stable to ensure that the assembly consists of only the designated molecules and configuration. The thermal and chemical stability of the synthesized framework, which are determined by the bonding strength between the participating molecules, are also important limiting factors. Lastly, it is critical to have a high level of control over the crystal growth process so that a consistent long-range order of the lattice structure can be realized.

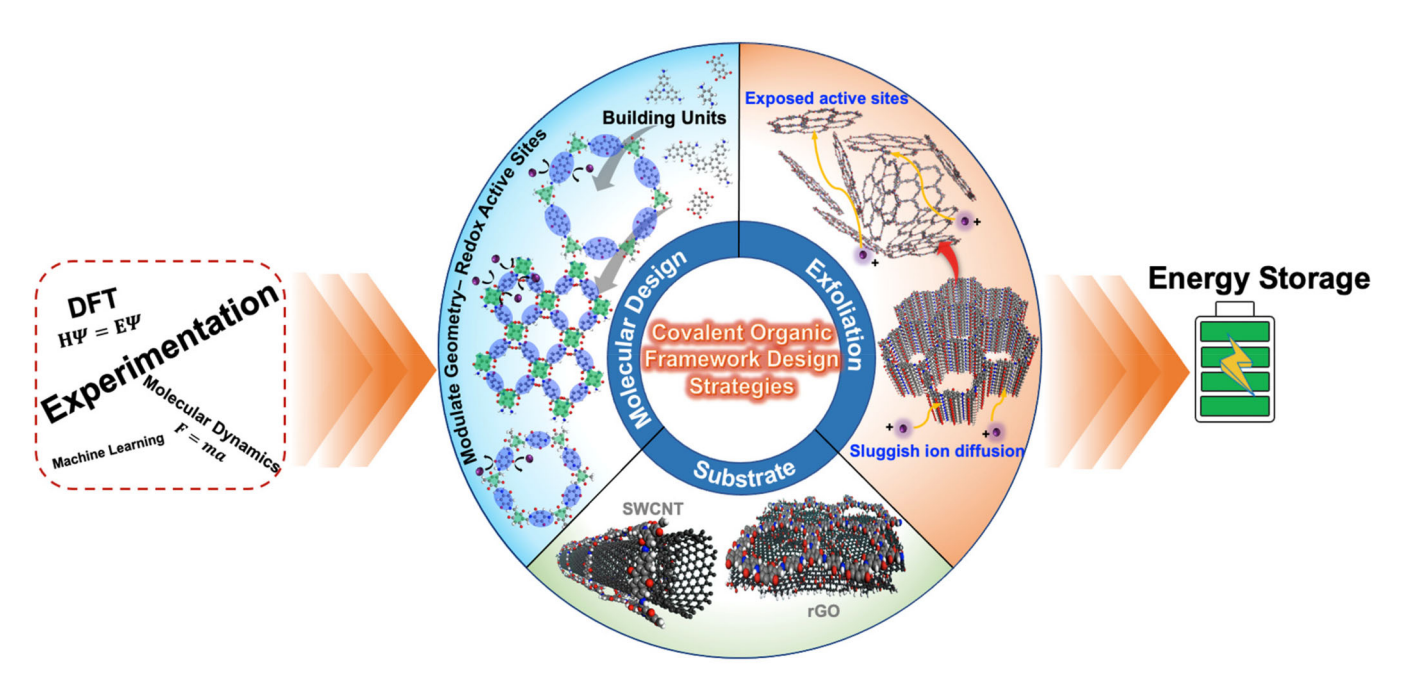


FIGURE 1 Schematic of major COF design strategies for energy storage applications

The geometric and compositional flexibility of COFs with the long-range structural order is particularly advantageous for designing functional materials because their properties can be precisely tuned according to the needs of the application. Since the discovery of feasible synthetic pathways, much effort has been devoted to exploring various aspects of the geometric complexity of COFs. Selected examples of recently reported COF building blocks for energy storage applications are shown in Figure 2. A series of characterization methods including Fourier-transform infrared spectroscopy (FTIR), X-ray photoelectron (XPS) spectroscopy, Raman spectroscopy, elemental analysis (EA) and solid-state nuclear magnetic resonance (NMR) spectroscopy have been employed to determine the chemical composition and structure of COFs. The morphology of COFs can be visualized using high-resolution transmission electron microscopy (TEM) and scanning electron microscopy (SEM). In addition, the crystalline structure of COF can be examined by X-ray diffraction (XRD) patterns, and thermogravimetric analysis (TGA) is commonly employed to evaluate thermal stability. Recent studies have also measured in situ Raman<sup>48</sup> and FTIR<sup>49-51</sup> spectra to monitor the structural evolution of COFs during electrochemical processes.

While most existing studies focus on the design and application of binary COFs (consisting of two building blocks alternating in the framework), ordered 2D heterostructures bearing different pore sizes and constituents can be readily achieved, which further expands the complexity

and functionality of the material. 52-54 The COF with two different covalent bonding formations was synthesized by Zeng and coworkers using an orthogonal reaction strategy. 52 Two building blocks, namely 4-formylphenylboronic acid (FPBA) and 1,3,5-tris(4-aminophenyl)-benzene (TAPB) was utilized in covalent bond formation. While the ditopic groups of FPBA can convert to boroxine rings at high temperature, aldehydes can generate imine groups in the presence of amino groups under similar reaction conditions, and the reactions do not interfere with each other (Figure 3A). Pang and colleagues also achieved the COF assemblies with two and three different pore sizes within the framework by alternating linkages (Figure 3B).<sup>53</sup> The condensation reaction between D<sub>2h</sub>-symmetric tetraamine and C<sub>2</sub>-symmetric dialdehyde leads to two-pore dimensions in the framework. The geometry can be further diversified by copolymerization with another C2-symmetric dialdehyde with different dimensions, and the geometrical variation can be confirmed by powder X-ray diffraction (PXRD) and pore size analysis. These studies demonstrate that the inclusion of diversified linker molecules and bonding strategies is critical for the development of functional materials beyond the current binary COFs and holds tremendous potential for the design of multifunctional materials.

COFs bonded with carbon–carbon linkages have also been an attractive subject due to the potential to obtain graphene-like properties such as superior electronic conductivity and bond strength.<sup>56,57</sup> While the irreversible nature of most carbon bonding reactions would lead to the

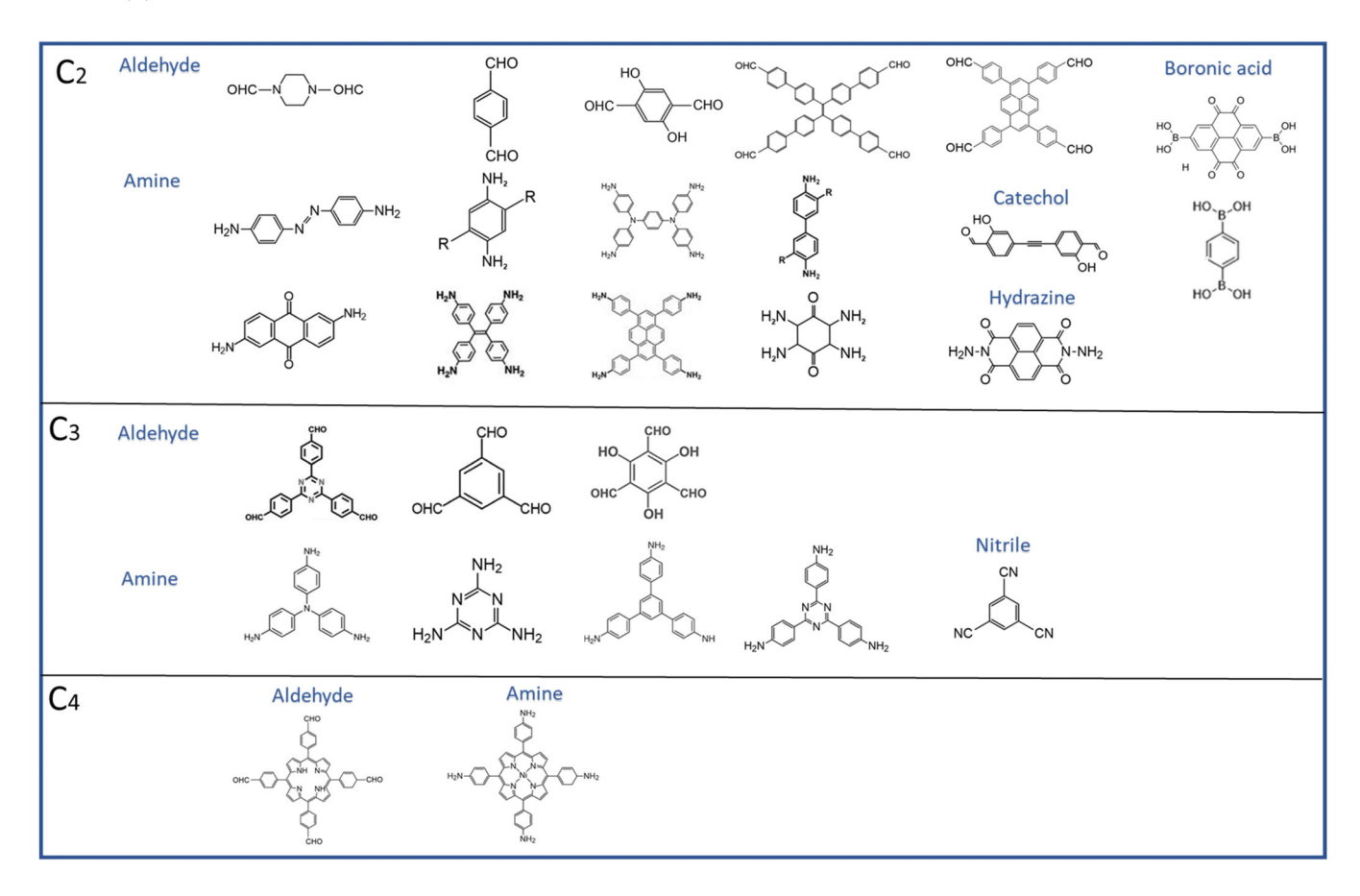
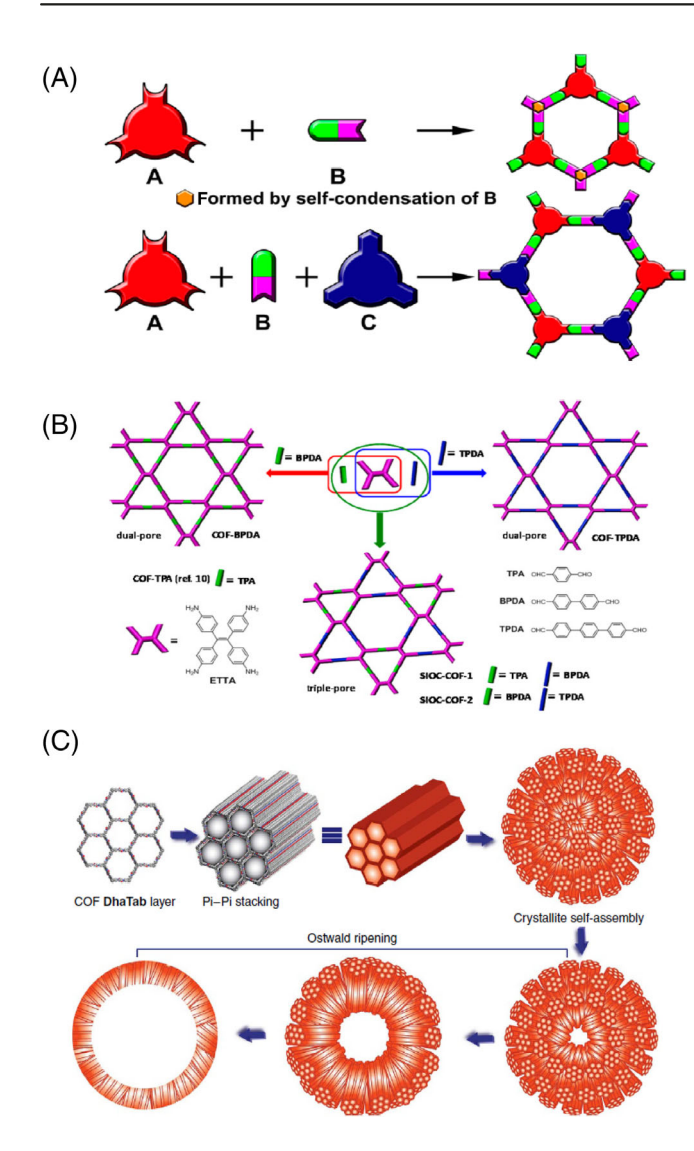


FIGURE 2 Geometries of common 2D COF building blocks for energy storage applications

formation of amorphous materials, as typically found in conjugated mesoporous polymers (CMPs), 58,59 recent studies have uncovered several feasible methods to synthesize crystalline carbon bond-based conjugated frameworks. 60,61 For example, Jin et al. demonstrated a 2D COF constructed from sp<sup>2</sup> carbon by C=C condensation reactions between tetrakis(4-formylphenyl)pyrene (TFPPy) and 1,4-phenylenediacetonitrile (PDAN).<sup>56</sup> The topologydirected polycondensation allows structural self-healing during the crystal growth process, while the pyrene unites serve as registry coordinates. The obtained sp<sup>2</sup>C-COF is a semiconductor that can be oxidized to enhance its conductivity. Another interesting phenomenon that could have a significant impact on the structure of COF is Ostwald ripening.55 In a time-dependent study on a COF (COF-DhaTab) formed using 2,5-dihydroxyterephthalaldehyde (Dha) and 1,3,5-tris(4-aminophenyl)benzene (Tab), the inside-out Ostwald ripening process was observed to transform COF-DhaTab from the conventional lamellar 2D  $\pi$ - $\pi$ stacking morphology to the hollow spherical structure (Figure 3C). The converted hollow spherical COF still maintained high crystallinity, porosity, surface area, and chemical stability owing to strong intramolecular hydrogen bonding.

#### 2.2 | Charge storage mechanism

To be employed as active materials for secondary energy storage devices, it is essential for COFs to undergoing reversible electrochemical redox reactions. Electroactive organic materials are typically divided into three categories (p-type, n-type, and bipolar) depending on their state of charge during the redox reaction.<sup>5,62</sup> N-type organic materials conduct redox reactions by accepting electrons in the neutral state to become negatively charged, followed by subsequent oxidation reactions back to the neutral state. On the other hand, the reaction for p-type organic materials is between the neutral state and the positively charged state. Bipolar organic materials are unique in that they can be either reduced to a negatively charged state or oxidized to a positively charged state, though typically the only one side of the reaction is utilized for charge storage applications. The electrochemical properties are determined by the type of redox centers where charge transfer takes place, and the charge storage mechanism of the COF electrodes primarily relies on the incorporation of organic redox-active moieties within the framework. For example, COFs containing quinones or imides are usually n-type electrodes because they have a



**FIGURE 3** Structural diversity of COFs. (A) Diagrams for the construction of binary and ternary COFs from orthogonal reaction strategy.<sup>52</sup> Reproduced with permission: Copyright 2015, American Chemical Society (further permissions related to the material excerpted should be directed to the ACS). (B) Representation for the synthesis of dual-pore and triple-pore COFs.<sup>53</sup> Reproduced with permission: Copyright 2016, American Chemical Society. (C) Proposed mechanism of the formation of COF hollow spheres.<sup>55</sup> Reproduced with permission: Copyright 2015, Springer Nature

conjugated carbonyl structure as the redox center.<sup>4,46</sup> Additionally, other charge storage mechanisms such as ion intercalation to the aromatic rings and electrical double layer capacitance (EDLC) can also be utilized to store charge in the COF electrodes.

Since the constituents of COFs generally retain their electrochemical properties after covalent bond formation, selective integration of redox-active molecules into the framework is the most convenient strategy for designing COF electrodes. For instance, TFP-DAAQ-COF, the first COF studied as a cathode material, was synthesized by

incorporating redox-active 2,6-diamino-anthraquinone (DAAQ) with 1,3,5-tris(4-formylphenyl)benzene (TFP) using covalent C-N bonds.63 While embedded in the framework, the bonded DAAQ molecules performed redox reactions similar to those of the monomer and polymer form. The drawback of this strategy is that most of the binary COFs can only incorporate one redox-active molecule using known reaction pathways due to the lack of compatible electroactive building blocks. Due to the limitation of linker selection, half of the molecules are electrochemically inactive, resulting in poor charge storage capacity. Although both TFP and DAAQ molecules contain carbonyl redox centers, it has been found that the ones within DAAQ have a redox potential of ~2.3 V versus Li/Li<sup>+</sup>, while the ones from TFP are less than 0.5 V versus Li/Li<sup>+</sup>.64,65 Therefore, designing COFs with higher redox activity within the suitable potential window and reaction condition is one of the most important topics for developing COF-based active materials.

#### 2.3 | Synthesis methods

Although crystalline organic materials had been actively pursued in the past, the difficulty of retaining crystallinity during polymerization hindered their realization. This obstacle has been addressed in the development of COFs, in which covalent bonds between light elements (B, C, O, H, N) can provide robust linkage and ordered structural pattern, allowing the formation of macroscopic organic solid without sacrificing crystallinity.8 In 2005, the first synthesis and crystallization of porous COF were demonstrated by the condensation reactions between phenyl diboronic acid and hexahydroxytriphenylene.<sup>7</sup> The synthesized COF maintained its crystal structure by strong covalent bonds with a rigid porous morphology and exhibits high thermal stability and surface area. All of these characteristics are commendable traits for a variety of applications such as gas storage, catalysis, and energy storage. 31,33,34 Following the initial report, COFs with different geometry and functionality have been developed through various reaction pathways, generally exhibiting higher chemical stability. 43,45 Despite the variations in composition and structure, COF design and synthesis approaches are generally consistent. As a necessary premise, the construction of COFs requires a target morphology that is feasible to assemble with a set of selected linker molecules. The potential linkage between the molecules should be examined to verify if the bond is (1) sufficiently strong to sustain a stable framework, (2) geometrically compatible to obtain a consistent longrange order, and (3) exhibit consistency and reversibility during the reaction under synthetic conditions.

The initial COF synthesis procedure focused on preserving the reversibility of the COF formation reaction, which is critical for eliminating structural error and maintaining the long-range order of the framework. Therefore, the syntheses of COFs were conducted in an inert environment to minimize interference during the solvothermal reaction over several days. This is the most common method for synthesizing COF as well as many COF-based composites with other conductive materials such as graphene and carbon nanotube (CNT).7,66 Controlled synthesis of 2D COF thin films on single-layer graphene was reported by Colson et al., where graphene was simply added to the mixture of COF constituent monomers prior to the solvothermal reaction.<sup>66</sup> While the solvothermal method can produce COF with consistent yield and high crystallinity, it is time-consuming, costly, and lacking in scalability. Therefore, it is important to develop more efficient and scalable synthesis methods suitable for mass production in industrial applications. Peng et al. demonstrated the synthesis of 2D COFs with imine, enamine, and azine linkages under ambient conditions that exhibit comparable crystallinity and porosity to their counterpart under solvothermal conditions.<sup>67</sup> The successful COF formation under mild synthetic conditions can be attributed to the high solubility of the linkers in the solvent and the strong  $\pi$ - $\pi$  stacking interactions between monomers and oligomers during formation. Evidently, building blocks with weaker  $\pi$ -stacking would result in COF products with much lower BET surface area and poor stability, indicating less favorable interlayer stacking and lower crystallinity. Synthesis of COFs with other geometries has also been demonstrated under ambient conditions, such as the solution-phase synthesis for spherical COF TpBD (a COF synthesized from TFP and benzidine [BD]) and ionothermal synthesis of 3D COFs containing ionic liquid. 64,68

Interfacial polymerization techniques have also been developed for the synthesis of COF films.<sup>69–71</sup> Freestanding COF films can be obtained by confining the reaction within a superspreading water layer between the oil and the hydrogel phase that contains the COF precursors.<sup>70</sup> The deposition of COF onto the substrate can also be achieved using a variety of methods.<sup>66,72,73</sup> Yang et al. recently reported self-controlled COF on Si/SiO2 substrate via a repolymerization process.<sup>72</sup> By charging both COF powder and the substrate in a Teflon-lined autoclave with the selected solvents and performing the solvothermal reaction, the COF powder gradually decomposes and reforms on the surface of the substrate at a self-established equilibrium state in the reversible polymerization–decomposition–repolymerization reaction.

In addition to solvothermal reactions and spontaneous reactions in the ambient atmosphere, methods

employing alternative gradients to accelerate the reaction process have also been studied. COFs synthesized using mechanochemical, 60 microwave, 74-76 sonochemical, 77 and vapor-assisted<sup>78</sup> methods have been reported. For example, Biswal et al. demonstrated a mechanochemical synthesis method for TpPa-1 (MC) and TpPa-2 simply by mechanical grinding (Figure 6A).60 Although the COF showed relatively low crystallinity, this method is much easier to perform than the solvothermal method, and the resulting COF layers were also simultaneously exfoliated. Another expedite method is to use the microwaveenergized reaction reported by Campbell and colleagues.<sup>74</sup> These studies reported processing time around 20-60 min, which are much faster compared to those using the conventional solvothermal method typically taking a few days. Overall, studies so far have shown that COFs can be successfully manufactured with facile procedures under less demanding laboratory conditions, but some accelerated methods may lead to reduced crystallinity of the framework, and compatibility of each method with a wider variety of COF assemblies still require further validation.

#### 3 | SUPERCAPACITORS

Supercapacitors are energy storage devices that output pulse currents to meet high power demand in a short period of time. The system bridges the performance gap between traditional capacitors and batteries in terms of having considerable power output as well as substantial energy storage capacity at the same time. Supercapacitors are suitable for a broad range of energy storage solutions including secondary power supply and excess energy supply/recovery systems (e.g., recover vehicle braking energy). There are two major types of charge storage mechanisms for COF supercapacitors: (1) electric charge accumulation on the electrode surface of EDLCs, and (2) pseudocapacitance originates from the surface redox reactions on the electrode material. The charge storage of EDLCs is carried out by the physical adsorption of electrolyte ions on the electrode surface in the absence of any chemical reaction, while pseudocapacitance relies on Faradic (redox) reactions in many metal oxides and various organic molecules. As the intermediate solution between batteries and capacitors, it is typical for high-performance supercapacitors to derive capacitance from both mechanisms. COF is considered a promising electrode material for supercapacitor applications owing to its unique crystalline porous structure enabling atomic-scale control of its structural component. The porous organic frameworks offer a high surface area preferable for EDLC as

well as convenient ion diffusion pathways for the electrolyte. The fact that the structural component can be controlled at the molecular level enables the purposeful design of the framework with redox-active moieties to provide pseudocapacitance. In principle, other critical parameters such as redox potential, electric conductivity, and thermal/chemical stability can be adjusted deliberately in a similar fashion. In many cases, rationally designed COF electrodes would possess superior electrochemical performance compared to their monomer building blocks. The stable structure also provides a great opportunity for incorporating other energy storage materials into the framework to further enhance its electrochemical performance. Analogous concepts are also applicable in other EES systems.

The first example of a COF electrode for capacitive energy storage is the β-ketoenamine-linked 2D COF (DAAQ-TFP COF) reported by DeBlase and coworkers in 2013, in which the COF was synthesized using redox-active anthraguinone moieties and 1,3,5-triformylphloroglucinol (TFP) via condensation reaction under solvothermal conditions (Figure 4).<sup>63</sup> The DAAQ-TFP COF electrode exhibited exceptional stability over 5000 cycles with a capacitance of  $48 \text{ F g}^{-1}$  at  $0.1 \text{ A g}^{-1}$ . The modest capacitance is likely due to the low accessibility of anthraquinone redox units for charge storage. In a later study, DAAQ-TFP COF was coated on the Au substrate for synthesizing crystalline, oriented thin films. Most of the anthraquinone groups (80%-99%) are electrochemically accessible in the films thinner than 200 nm, resulting in a significant increase in capacitance.<sup>79</sup> This result highlights the importance of ion transport to the redox-active sites by structural optimization. Additionally, the capability of COFs to interact with

various ions such as K<sup>+</sup>, Li<sup>+</sup>, and Mg<sup>2+</sup> in their reduced forms was verified by examining the framework incorporating naphthalene diimides (NDI) and TFP.<sup>80</sup> In recent years, many COF studies regarding aspects of molecular design, composite material, and structural optimization strategies such as layer alignment and exfoliation have been reported with promising prospects.

#### 3.1 | Molecular structure of COFs

Various redox-active COFs have been studied, as detailed in Table 1. For example, Xu et al. developed a general strategy to introduce redox-active molecules into conventional COF via postsynthesis functionalization with organic radicals.<sup>89</sup> The synthesized COF consists of nickel porphyrin at the vertices and ethynyl units on the electrochemically inactive channel. The ethynyl groups underwent click reaction with 4-azido-2,2,6,6-tetramethyl-1-piperidinyloxy to yield [TEMPO]-NiP-COF, exhibiting capacitance as high as 167 F g<sup>-1</sup> at 0.1 A g<sup>-1</sup> and 113 F  $g^{-1}$  at 2 A  $g^{-1}$ . A nitrogen-rich, triazine-based framework was synthesized by Hao et al. to study the effect of heteroatomic doping and micropore structure, and exhibited a capacitance of 150 F g<sup>-1</sup> at 0.1 A g<sup>-1,81</sup> Triphenylamine based COF has also recently been investigated by El-Mahdy and colleagues.<sup>82</sup> The two synthesized COFs were composed of redox-active TPPDA(NH<sub>2</sub>)<sub>4</sub> tetraformyl linkers, TPPvr(CHO)<sub>4</sub>, TPTPE(CHO)<sub>4</sub>. Because of the presence of heteroatoms, larger pore size (0.82 cm<sup>3</sup> g<sup>-1</sup>), and high surface area over 1000 m<sup>2</sup> g<sup>-1</sup>, the specific capacitance of the TPPDA-TPTPE COF (237.1 F g<sup>-1</sup>) was larger than that of the

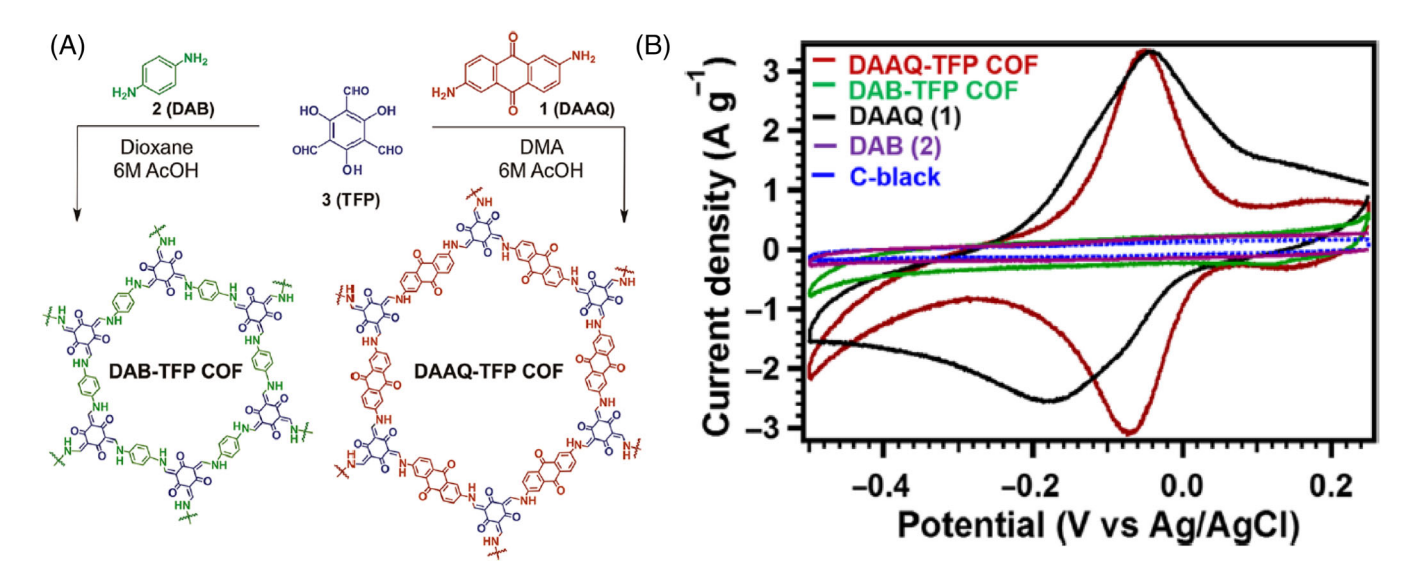


FIGURE 4 (A) Synthesis of DAB- and DAAQ-TFP-COF and (B) their cyclic voltammograms (50 mV s<sup>-1</sup>, 1 M H<sub>2</sub>SO<sub>4</sub> supporting electrolyte) comparing to the active monomer molecules.<sup>63</sup> Reproduced with permission: Copyright 2013, American Chemical Society

**TABLE 1** Electrochemical performances of representative COF-based supercapacitors

COF	Composite/ substrate	Electrolyte	Current density	Specific capacitance	Cycling stability [# of cycles] (current density)	Cycling retention (%)
DAAQ-TFP COF <sup>63</sup>	_	1 M H <sub>2</sub> SO <sub>4</sub>	$0.1~{\rm A~g^{-1}}$	$48 \; \mathrm{F} \; \mathrm{g}^{-1}$	$5000 (0.1 \text{ A g}^{-1})$	83
DAAQ-TFP-COF film <sup>79</sup>	-	$1 \text{ M H}_2\text{SO}_4$	$150 \ \mu A \ cm^{-2}$	$3 \text{ mF cm}^{-2}$	5000 (150 μA cm <sup>-2</sup> )	93
$\mathrm{PTF}^{81}$	_	EMIMBF <sub>4</sub>	$0.1~{\rm A~g}^{-1}$	$151.3~{\rm F~g^{-1}}$	$10\ 000\ (10\ { m A\ g}^{-1})$	85
TPPDA-TPPyr <sup>82</sup>	_	1 M KOH	$2~\mathrm{A~g}^{-1}$	$188.7~{\rm F~g^{-1}}$	$5000 (10 \text{ A g}^{-1})$	85.6
TPPDA-TPTPE <sup>82</sup>	_	1 М КОН	$2~\mathrm{A~g}^{-1}$	$237.1~{\rm F~g^{-1}}$	$5000 (10 \text{ A g}^{-1})$	86.2
TaPa-Py COF <sup>83</sup>	_	$1 \text{ M H}_2\text{SO}_4$	$0.5~{\rm A~g^{-1}}$	$209~\mathrm{F~g^{-1}}$	$6000 (2 \text{ A g}^{-1})$	92
Dq1Da1Tp COF <sup>84</sup>	_	$1 \text{ M H}_2\text{SO}_4$	$1.56~\mathrm{mA~cm^{-2}}$	$111~\mathrm{F~g^{-1}}$	2500 (0.39 mA cm <sup>-2</sup> )	90
TpPa-(OH) <sub>2</sub> <sup>85</sup>	_	1 M phosphate buffer (pH = 7.2)	$0.5~{ m A~g}^{-1}$	416 F g <sup>-1</sup>	10 000 (5 A g <sup>-1</sup> )	88
TpOMe-DAQ <sup>86</sup>	_	3 M H <sub>2</sub> SO <sub>4</sub>	$3.3 \text{ mA cm}^{-2}$	$1600 \text{ mF}$ $\text{cm}^{-2}$ $169 \text{ F g}^{-1}$	100 000 (10 mA cm <sup>-2</sup> )	>100
$PDC - MA - COF^{87}$	_	6 M KOH	$1~{\rm A~g^{-1}}$	$335~\mathrm{F~g^{-1}}$	$20\ 000\ (5.0\ A\ g^{-1})$	88
Exfoliated JUC-512 <sup>88</sup>	_	1 M NBu <sub>4</sub> PF <sub>4</sub> / ACN	$1000~\mathrm{mV~s^{-1}}$	5.85 mF cm <sup>-2</sup>	10 000 (1000 mV s <sup>-1</sup> )	~100
NiP-COF <sup>89</sup>	TEMPO	(C <sub>4</sub> H <sub>9</sub> ) <sub>4</sub> NClO <sub>4</sub>	$0.1~{ m A~g^{-1}} \ 2~{ m A~g^{-1}}$	$167 \text{ F g}^{-1}$ $113 \text{ F g}^{-1}$	$100 (0.5 \text{ A g}^{-1})$	100
DAAQ-TFP-COF <sup>90</sup>	PEDOT	0.1 M (n- Bu) <sub>4</sub> NClO <sub>4</sub> (TBAP)	10 C 1600 C	350 F cm <sup>-3</sup> 175 F cm <sup>-3</sup>	10 000 (100 C)	>100
AQ-COF <sup>91</sup>	PEDOT	$1 \text{ M H}_2\text{SO}_4$	$1~{ m A~g}^{-1}$	$1663~{\rm F~g^{-1}}$	$10\ 000\ (50\ \mathrm{A\ g}^{-1})$	>100
TpPa-COF <sup>92</sup>	Polyaniline	$1 \text{ M H}_2\text{SO}_4$	$0.2~\mathrm{A~g}^{-1}$	$95~\mathrm{F~g^{-1}}$	$30\ 000\ (5\ A\ g^{-1})$	83
TpPa-COF <sup>93</sup>	Nickel nanowire	1 M LiCl	$2 \text{ A g}^{-1}$ $50 \text{ A g}^{-1}$	424 F g <sup>-1</sup> 314 F g <sup>-1</sup>	2500 (20 A g <sup>-1</sup> )	>100
COFTTA-DHTA <sup>94</sup>	NH2-f- MWCNT	1 M Na <sub>2</sub> SO <sub>4</sub>	$0.4 \text{ A g}^{-1}$ $2 \text{ A g}^{-1}$	$127.5 \text{ F g}^{-1}$ $98.7 \text{ F g}^{-1}$	1000	96
g-C34N6-COF <sup>95</sup>	CNT	LiCl/PVA gel	$2 \text{ mV s}^{-1}$ 500 mV s <sup>-1</sup>	15.2 mF cm <sup>-2</sup> 5.1 mF cm <sup>-2</sup>	5000 (2 mA cm <sup>-2</sup> )	93.1
COFDAAQ-BTA <sup>96</sup>	3D graphene	1 М КОН	$0.025 \text{ mA cm}^{-2}$	31.7 mF cm <sup>-2</sup>	2500 (0.5 mA cm <sup>-2</sup> )	30
COFBTA-DPPD <sup>97</sup>	rGO	2 M KOH	$0.5 \text{ A g}^{-1}$ $2 \text{ A g}^{-1}$	239.1 F g <sup>-1</sup> 158.1 F g <sup>-1</sup>	1500 (0.5 A g <sup>-1</sup> )	70
TFB-DAB COF <sup>98</sup>	NH2-rGO	1 M Na <sub>2</sub> SO <sub>4</sub>	$0.2~\mathrm{A~g^{-1}}$	$533~\mathrm{F~g}^{-1}$	1000	79
TpDp-COF <sup>99</sup>	rGO	0.5 M H <sub>2</sub> SO <sub>4</sub>	$0.5 \text{ A g}^{-1}$ $10 \text{ A g}^{-1}$	269 F g <sup>-1</sup> 222 F g <sup>-1</sup>	5000 (8 A g <sup>-1</sup> )	96
DAAQ-COF <sup>100</sup>	Graphene aerogel	$1 \text{ M H}_2\text{SO}_4$	$1~\mathrm{A~g^{-1}}$	$378 \; \mathrm{F} \; \mathrm{g}^{-1}$	20 000 (15 A g <sup>-1</sup> )	87.8
ILCOF-1 <sup>101</sup>	rGO	1 M H <sub>2</sub> SO <sub>4</sub>	1 A g <sup>-1</sup>	321 F g <sup>-1</sup> 237 F cm <sup>-3</sup>	20 000 (N/A)	88

TPPDA-TPPyr COF (188.7 F  $g^{-1}$ ) at a current density of 2 A  $g^{-1}$ . 2D COF with redox-active pyridine units was first synthesized by Khattak and colleagues, achieving a

capacitance  $\sim\!210~{\rm F~g}^{-1}$  at a low current density of 0.5 A g $^{-1}$  as well as good rate-performance and cycling stability. More recently, COFs with pyridyl-lined

micropores have been synthesized by Haldar and coworkers to investigate the effects of varying chemical functionality. 102 The framework was assembled using tripyridine-triazine amine and trialdehydes containing one to three hydroxyl groups. This study revealed that structural and chemical properties such as stacking patterns, hydrogen bonding interactions, and the redox potential can be systematically modified by structural adjustment at the atomic level. Hence, the combination of EDLC and pseudocapacitance was optimized using such a strategy and delivered excellent specific capacitance of 546 F g<sup>-1</sup> at  $0.5 \text{ A g}^{-1}$  and 95% capacity retention after 10 000 cycles. In addition, introducing hybrid building blocks is a novel strategy that could effectively modify the mechanical and chemical properties of the COF. Khayum et al. designed a heterolinked COF using both 2,6-diaminoanthraquinone (Dg) and 2,6-diaminoanthracene (Da) as interchangeable building blocks to bind with TFP via solid-state molecular baking strategy (Figure 5).84 While Dq is electrochemically

active in redox reactions, Da improves the mechanical robustness of the hetero-linked COF due to the enhanced noncovalent interaction between crystallites, yielding a porous, crystalline, flexible, and free-standing supercapacitor electrode. The mechanically robust  $Dq_1Da_1Tp$  COF thin film (Da:Dq 1:1) exhibited a fair specific capacitance of 111 F g<sup>-1</sup> at 1.56 mA cm<sup>-2</sup>.

Owing to their crystal structure, controlled functionalization, and accurate atomic-scale measurement capability, redox-active COFs also offer a unique opportunity to explore long-range hydrogen bonding interactions in organic material and utilize the favorable properties originating from them, such as enhanced crystallinity and chemical stability. The role of intramolecular hydrogen bonding in COFs was reported by Chandra et al., in which TpPa-(OH)<sub>2</sub> was synthesized by the Schiff base condensation between 1,3,5-triformylpholoroglucinol (TFP) and 2,5-dihydroxy-1,4-phenyldiamine [Pa-(OH)<sub>2</sub>] under solvothermal conditions, and was subsequently

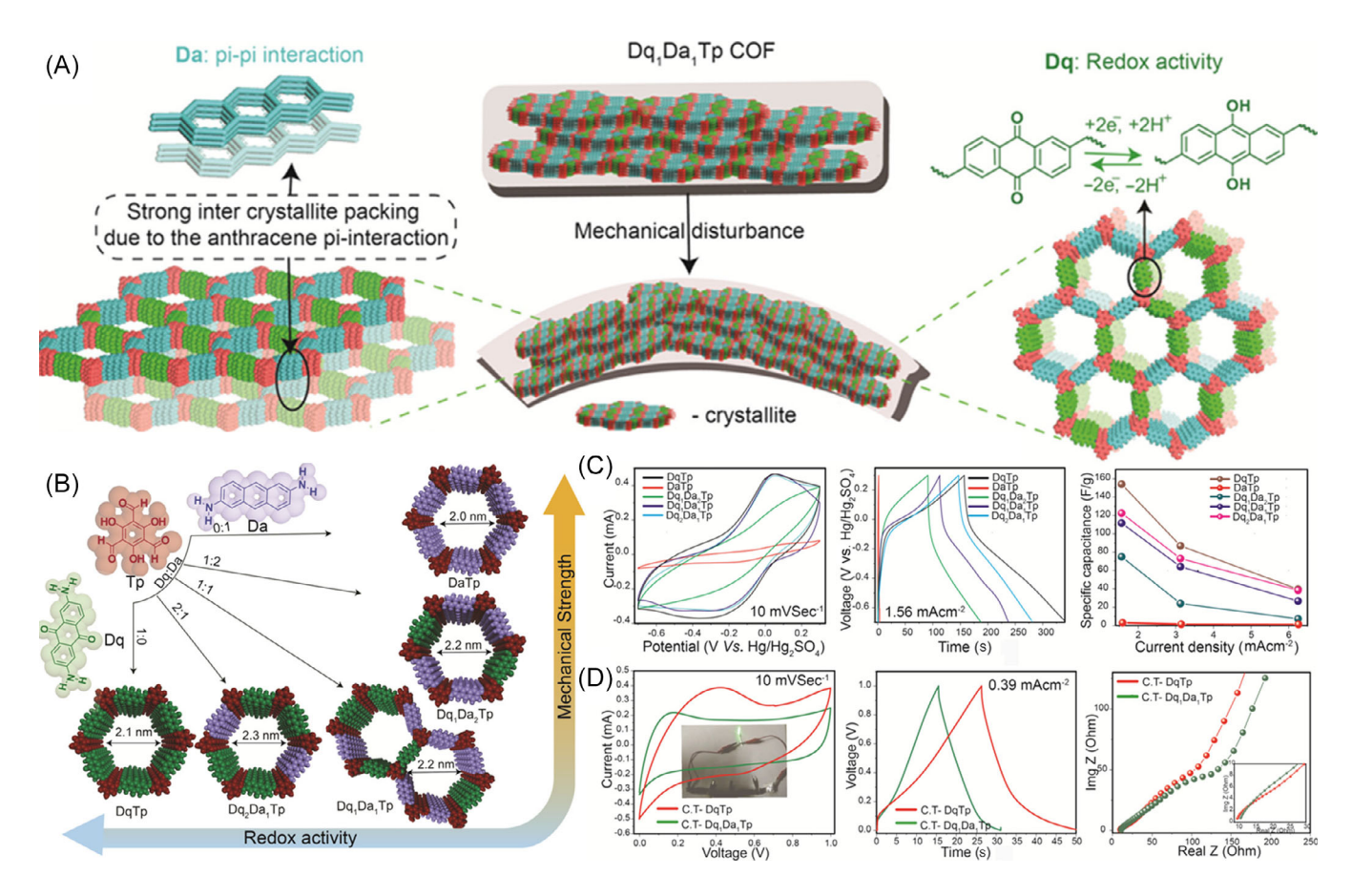


FIGURE 5 (A) Hybrid property of Dq1Da1Tp COF thin sheet. (B) Schematic representation of the synthesis of hybrid COF (Dq-2,6-diaminoanthraquinone, Da-2,6-diaminoanthracene, and Tp-1,3,5 triformylpholoroglucinol). (C) Three-electrode characterization using CV and charge–discharge (CD), and the plot represents current density versus specific capacitance. (D) Device characterization: CV (inset: 3.5 V LED lighted up by the series connection of four flexible devices), CD, and impedance analysis of CT-Dq1Da1Tp COF supercapacitor devices. (B) Schematic representation of the synthesis of hybrid COF (Dq-2,6-diaminoanthraquinone, Da-2,6-diaminoanthracene, and Tp-1,3,5 triformylpholoroglucinol). (C) Three-electrode characterization using CV and charge–discharge (CD), and the plot represents current density versus specific capacitance. (D) Device characterization: CV (inset: 3.5 V LED lighted up by the series connection of four flexible devices), CD, and impedance analysis of CT-Dq1Da1Tp COF supercapacitor devices. (D) Device characterization: CV (inset: 3.5 V LED lighted up by the series connection of four flexible devices), CD, and impedance analysis of CT-Dq1Da1Tp COF supercapacitor devices. (D) Device characterization: (D)

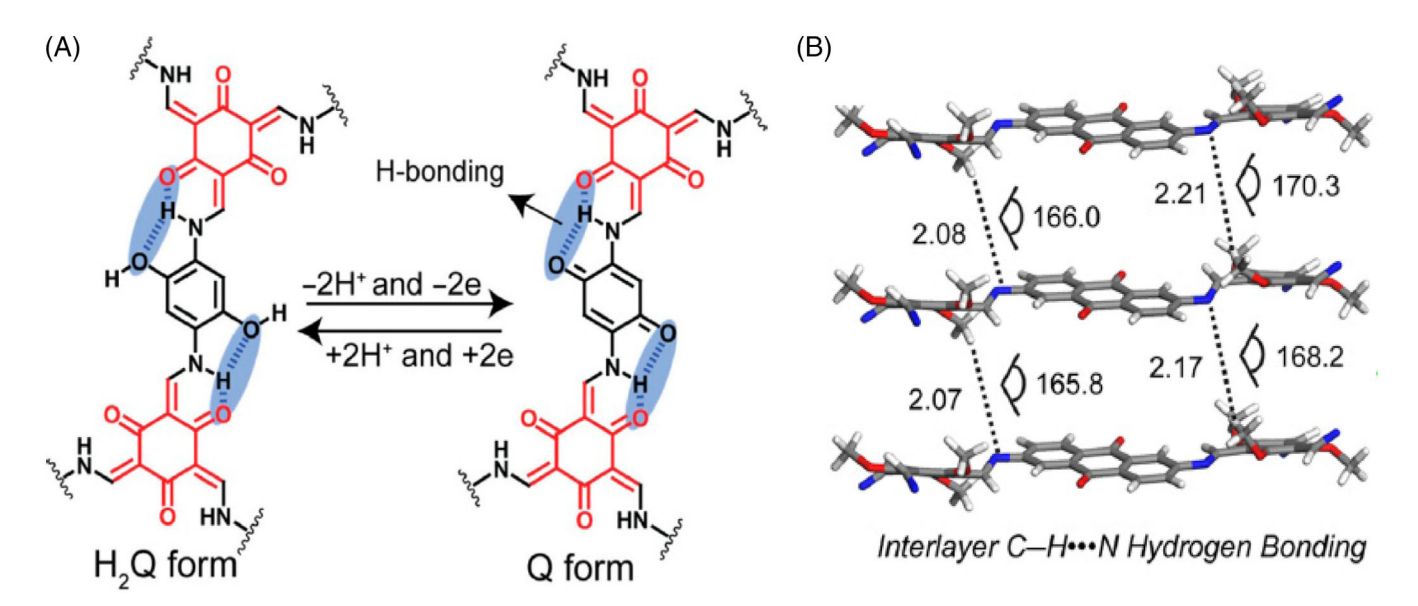


FIGURE 6 Schematic of hydrogen bond interactions in COF. (A) Intralayer H-bonding for hydroquinone and benzoquinone. 85 Reproduced with permission: Copyright 2017, American Chemical Society. (B) Interlayer C—H···N H-bonding in TpOMe-DAQ based on distances (H to N atom; Å) shown with dotted line and angles (C—H···N) in degree. 86 Reproduced with permission: Copyright 2018, American Chemical Society

compared with the COFs functionalized with phenolic and methoxy groups as well as their nonfunctionalized counterparts. The phenol functionalized COF exhibited modest initial capacitance of 86 F g at 20 mV s $^{-1}$  scan rate in CV measurement, but quickly diminished due to the decomposition of phenoxy radicals. However, benzoquinone did not decompose as expected and exhibited reversible redox activity over extended cycling, which can be attributed to the hydrogen bonding interaction between the carbonyl oxygen of the benzoquinone functionality with the neighboring amine group reinforcing the framework (Figure 6A). The H-bonding interaction can suppress the decomposition of hydroquinone and sustain 88% capacitance retention after 10 000 cycles at 0.8 A g $^{-1}$ .

In addition to intra-layer interactions, hydrogen bonding can also play a critical role in shaping the interlayer stacking characteristics. Halder et al. synthesized a stable freestanding supercapacitor electrode using 2,4,6-trimethoxy-1,3,5-benzenetricarbaldehyde (TpOMe) and 2,6-diaminoanthraquinone (DAQ) as building blocks.<sup>86</sup> The TpOMe-DAQ framework exhibited an exceptional areal capacitance of 1600 mF cm<sup>-2</sup> owing to its large surface area (1734 m<sup>2</sup> g<sup>-1</sup>). More importantly, the framework possesses ultrahigh chemical stability due to the presence of interlayer C-H...N hydrogen bond between methoxy C-N and the imine nitrogen atom of adjacent layers as shown in Figure 6B, which could withstand extremely acidic and alkaline environments (18 M H<sub>2</sub>SO<sub>4</sub>/9 M NaOH). Li et al. studied similar C-H···N hydrogen bond interactions using a triazine-based COF consisting of 1,4-piperazinedicarboxaldehyde (PDC) and melamine (MA).<sup>87</sup> It was found that the interlayer C—H···N hydrogen bond can "lock" the relative distance between two adjacent layers to avoid interlayer slipping, hence maintaining the ordered pore structure of COF and improving charge transfer between the electrode interface and triazine units. The analogous conclusion was also reached by Haldar and coworkers in their aforementioned study, in which the presence of more hydroxyl groups gave rise to stronger interlayer hydrogen bonds and resulted in a denser ABAB stacking pattern with higher packing efficiency.<sup>102</sup>

#### 3.2 | Exfoliation of COFs

Although redox-active COFs could be employed as active materials for energy storage devices, most COF electrodes failed to reach the performance parameters to be considered sufficiently competitive with other organic/inorganic candidates as they have three major flaws: (1) the capacitance is relatively low because most existing linker molecules are not redox-active, and therefore about half of the molecules cannot be utilized in charge storage applications; (2) the electric conductivity is relatively low even in the conjugated crystalline structure, and requires large amounts of carbon additive in the electrode, further reducing the energy storage capacity in cell assembly; and (3) the utilization of redox-active sites is still relatively low in bulk structures due to the restricted

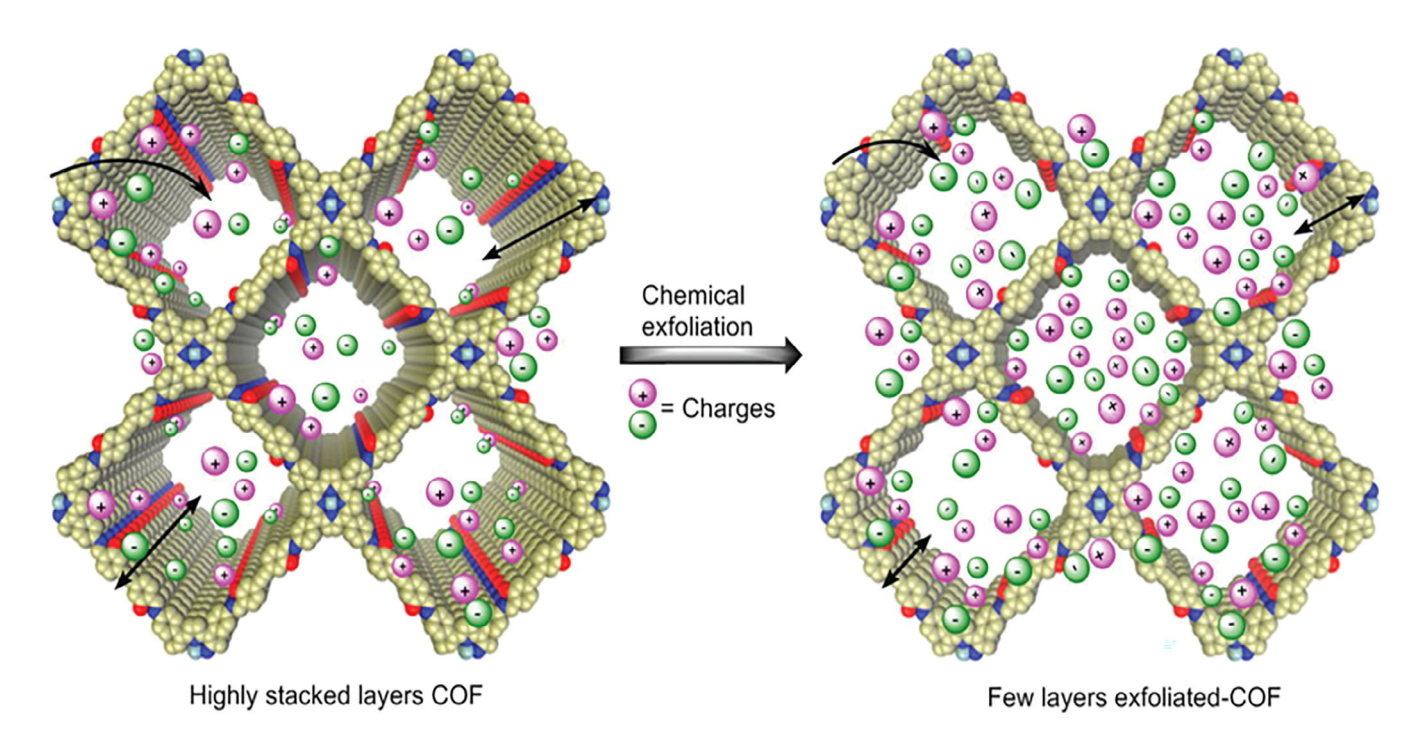


FIGURE 7 Schematic of difference in ion transport between bulk and exfoliation COFs. 88 Reproduced with permission: Copyright 2020, John Wiley and Sons

diffusion pathways within the nanochannels. Various strategies have been proposed aiming to solve those issues. Breakthrough results had been achieved by studying the exfoliated COFs via mechanical grinding, where exfoliation has been shown to significantly improve the electrochemical performance of COF for LIBs by shortening the ion diffusion path and shifting to charge transfer dominated process. 65 Following the report, further research regarding exfoliated COFs was conducted for supercapacitor systems as well. Yusran et al. synthesized the exfoliated mesoporous 2D COFs (e-COF) via a mild chemical exfoliation method to obtain an average thickness of 22 nm (Figure 7).88 The e-COF-based supercapacitor delivered superior areal capacitance (5.46 mF cm<sup>-2</sup> at 1000 mV s<sup>-1</sup>) and gravimetric power (55 kW kg<sup>-1</sup>) compared to the conventional capacitor and graphitic-carbon microcapacitors (typically  $<4 \text{ mF cm}^{-2} \text{ at } 1000 \text{ mV s}^{-1} \text{ and } <45 \text{ kW kg}^{-1}$ ).

# 3.3 | Composite electrodes with conductive substrates

Synthesizing hybrid electrodes with highly conductive nanocarbons such as CNT and graphene is another promising solution to mitigate the poor electric conductivity of COF electrodes and brings additional benefits such as enhanced surface area, hierarchal porosity by in-plane cavities, and controlled synthesis of few-layer COFs. 94-101 For instance, Sun et al. synthesized a highly crystalline COF with 4,4',4"-(1,3,5-triazine-2,4,6-triyl) trianiline (TTA) with 2,5-dihydroxyterepthaldehyde (DHTA) on amino-functionalized multi-walled CNT (NH2-f-MWCNT) via in situ polymerization method (Figure 8A). 94 Owing to the desirable combination of high crystallinity, surface area, chemical stability, and electric conductivity, the combination of conductive MWCNTs and crystalline porous COF<sub>TTA-DHTA</sub> electrode showed superior electrochemical performance (127.5 F g<sup>-1</sup> at 0.4 A g<sup>-1</sup>) compared to either of its components. Similar approaches were also taken with graphene/reduced graphene oxide (rGO) to take advantage of the synergetic effect. Wang et al. synthesized a composite electrode with imine-linked COFs as dispersed nano-deposits on amine-functionalized rGO substrate (Figure 8B).98 The resulting COFs/NH2-rGO electrode achieved a high capacitance of 533 F g<sup>-1</sup> at 0.2 A g<sup>-1</sup> with 79% retention after 1000 cycles in 1 M Na<sub>2</sub>SO<sub>4</sub>. By incorporating a nonredox-active COF into the COF/rGO hybrid electrode system, Wang et al. also investigated the impact of COF on the 3D rGO structure. 101 The synthesized imine-linked mesoporous 2D COF (ILCOF-1) nanosheets enable the physical separation of rGO layers as well as enhanced electrolyte ion transport through the mesopores. The rGO/COF hybrid electrode with 20% COF was able to deliver high specific capacitance of 321 F g<sup>-1</sup> and 237 F cm<sup>-3</sup> at 1 A g<sup>-1</sup>, which are 55% and ~45% better than those of the rGO electrode.

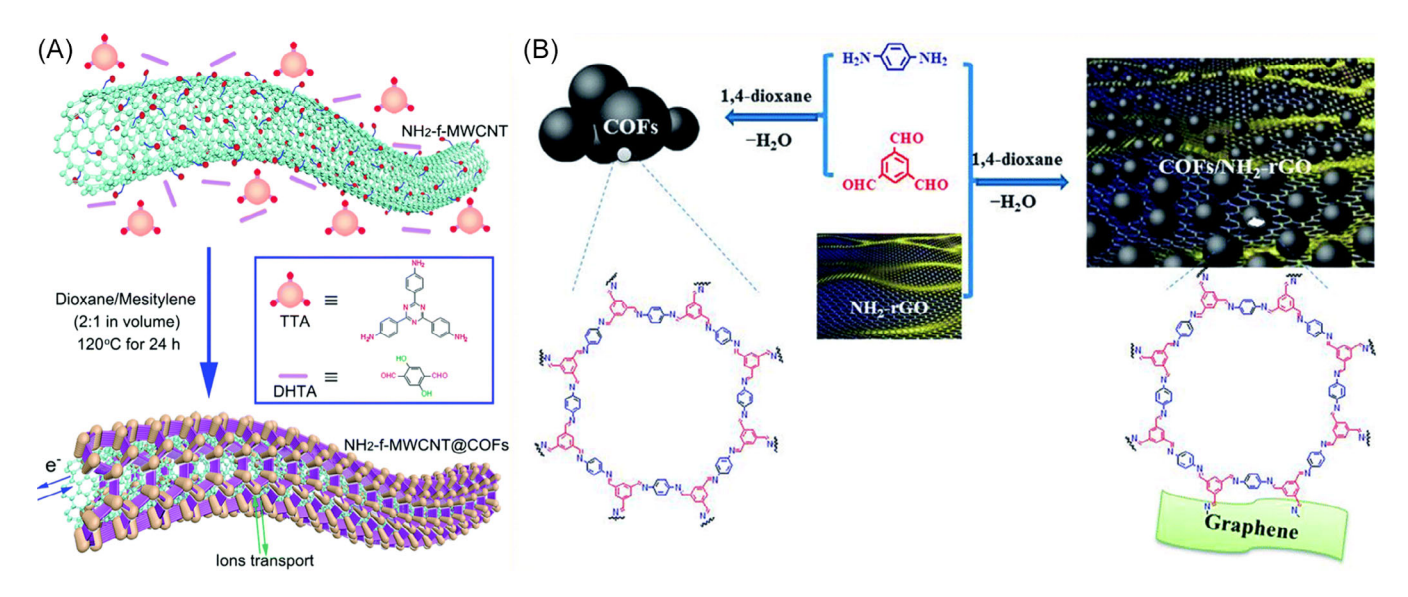
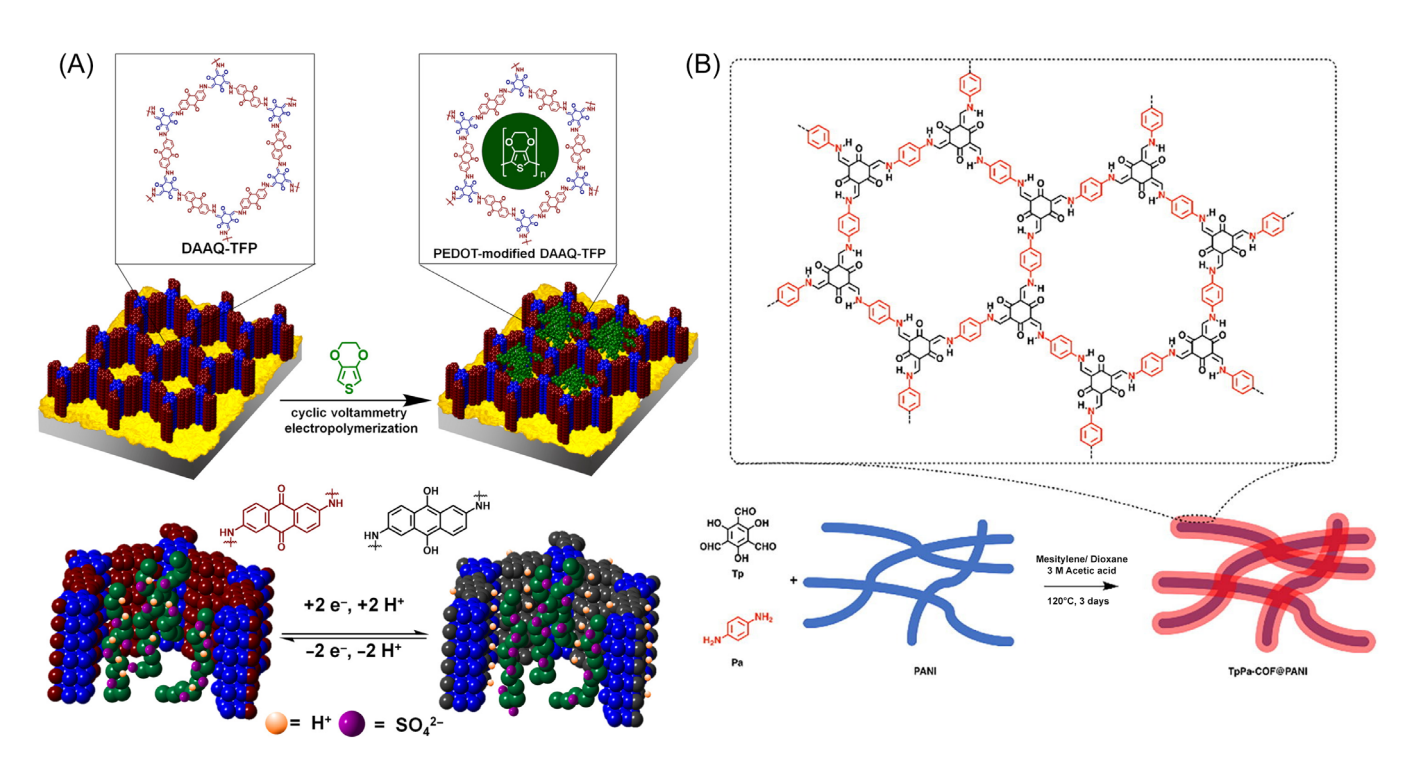


FIGURE 8 Schematic of COF hybrid electrode with (A) NH<sub>2</sub>-f-MWCNT<sup>94</sup> and (B) NH<sub>2</sub>-rGO.<sup>98</sup> Reproduced with permission: Copyright 2017, Royal Society of Chemistry.<sup>94</sup> Reproduced with permission: Copyright 2015, Royal Society of Chemistry.<sup>98</sup>



**FIGURE 9** (A) Depiction of modification of DAAQ-TFP films by electropolymerization of 3,4-ethylenedioxythiophene (EDOT) and the cross-section of a pore following the oxidation and reduction of the DAAQ moieties. Paperoduced with permission: Copyright 2016, American Chemical Society (further permissions related to the material excerpted should be directed to the ACS). (B) Schematic of synthesis of TpPa-COF@PANI in form of external COF coating. Paperoduced with permission: Copyright 2019, Elsevier

In addition to carbon nanomaterials, the integration of COF with conductive polymers has been investigated. Mulzer et al. enhanced the electrical conductivity of DAAQ-TFP-COF by electropolymerizing 3,4-ethylenedioxythiophene (EDOT) within the COF nanopore (Figure 9A). <sup>90</sup> Electropolymerization of EDOT significantly improved

electrochemical performance including high charging rate (10–1600 C) and impressive areal capacitance (~350 F cm $^{-3}$  at 10 C) in the relatively thick COF films (~1  $\mu m)$  by providing better electron access to the bulk redox-active carbonyl groups. The intra-pore modification strategy is critical in enhancing the volumetric energy density of COF-based

electrodes, which has been an innate flaw for pristine COFs due to their low packing density in exchange for the porous framework. This concept was further supported by Wu et al. using a more scalable in-situ solid-state polymerization method.<sup>91</sup> The COF composite electrode was synthesized with polyaniline (PANI)<sup>92</sup> and metal nanowire<sup>93</sup> using an in-situ polymerization method, resulting in a similar structure to the aforementioned CNT composite and improved electrochemical performance as well (Figure 9B).

#### 4 | SECONDARY BATTERIES

Conventional organic battery electrodes commonly suffer from slow ion diffusion, low electrical conductivity, and poor cycling stability.<sup>2,6</sup> Therefore, after the initial study on redox-active COFs and their potential as capacitive energy storage devices, the prospect of utilizing the reversible redox

charge storage mechanism in metal-ion battery systems has also attracted a great deal of attention. Similar in concept and design to supercapacitors, the development of COF battery electrodes revolves around approaches of bulk delamination and hybrid composite with other conductive materials such as nanocarbons and conductive polymers to enhance their ion diffusion kinetics and conductivity. While research on COF electrode materials is still in its early stages, many impressive electrochemical performances have been reported (summarized in Table 2) as a promising class of electrode materials for next-generation organic batteries.

#### 4.1 | Lithium-ion batteries

The first COF-based LIB electrode was demonstrated by Xu et al. in 2015. The redox-active  $D_{TP}$ - $A_{NDI}$ -COF consisting of 2,3,6,7,10,11-hexahydoxytriphenylene and N9-di(4-boronophenyl)-naphthalene-1,4,5,8-tetracarboxylic

TABLE 2 Electrochemical performances of representative COF-based Li/Na-ion electrodes

COF	Composite/ substrate	Potential window (V)	Current density (A g <sup>-1</sup> )	Specific capacity (mAh g <sup>-1</sup> )	Cycling stability [# of cycles] (currentdensity)	Cycling retention (%)	Theoretical capacity (mAh g <sup>-1</sup> )
DAAQ-ECOF <sup>65</sup>	_	1.5-4	0.02	145	1800 (0.5 A g <sup>-1</sup> )	98	151
DTP-ANDI-COF <sup>105</sup>	_	1.5-3.5	0.2	69	$700 (0.2 \text{ A g}^{-1})$	~100	83.3
Tp-DANT-COF <sup>106</sup>	_	1.5-4	0.05	104.3	600 (1.1 A g <sup>-1</sup> )	68.7	134
DAPO-TpOMe- COF <sup>107</sup>	_	1.5-4.2	0.1	81.9	200 (0.1 A g <sup>-1</sup> )	79	77
PDI-Tc <sup>108</sup>	_	1.75-3.25	0.00482	75.9	500 (0.193 A g <sup>-1</sup> )	80.2	96.4
PIBN <sup>50</sup>	Graphene	1.5-3.5	0.1 10	271 193.1	$300 (0.28 \text{ A g}^{-1})$	86	280
PI-ECOF <sup>109</sup>	rGO	1.5-3.5	0.0142	167	$300 (0.128 \text{ A g}^{-1})$	71	142
2D-PAI <sup>110</sup>	CNT	1.5-3.5	0.2	104.4	$8000 (0.5 \text{ A g}^{-1})$	100	126
2D PPTODB <sup>111</sup>	CNT	1.5-3.5	0.1	198	$150 (0.02 \text{ A g}^{-1})$	68.3	142
TQBQ-COF <sup>49</sup> (Na)	_	0.8-3.8	0.02	452	$1000 (1 \text{ A g}^{-1})$	96	515
$TThPP^{112}$	_	0-3	0.2	666	$1000 (0.4 \text{ A g}^{-1})$	61.1	686
N-COF <sup>113</sup>	_	0-3	0.2	806	$500 (1 \text{ A g}^{-1})$	81	N/A
PAT <sup>114</sup>	_	0-3	0.2	1770	$400 (1 \text{ A g}^{-1})$	>100	1450
Tp-Azo-COF <sup>51</sup>	_	0-3	0.1	529.5	$3000 (1 \text{ A g}^{-1})$	~100	577
IISERP-COF <sup>115</sup>	_	0-3	0.1	790	$720 (0.1 \text{ A g}^{-1})$	100	701
CTF-1 <sup>116</sup>	_	0-3	0.1	816	$500 (1 \text{ A g}^{-1})$	70.2	N/A
E-TFPB-COF <sup>117</sup>	_	0-3	0.1	1359	$300 (0.1 \text{ A g}^{-1})$	71.20	N/A
BTCA-DAB <sup>48</sup>	CNT	0-3	0.1	1536	$500 (0.1 \text{ A g}^{-1})$	66.5	1830
2D-CAP <sup>57</sup> (Na)	_	0-2.5	0.1	216	$7700 (5 \text{ A g}^{-1})$	70	N/A
DAAQ-COF <sup>118</sup> (Na)	_	0-3	0.1	420	$10\ 000\ (5\ A\ g^{-1})$	99	302
CON-16 <sup>119</sup> (Na)	_	0-2.5	0.1	250	$100 (0.3 \text{ A g}^{-1})$	69	360
Aza-COF <sup>120</sup> (Na)	_	0-3	0.06	550	$500 (3 \text{ A g}^{-1})$	87	603

acid diimide was synthesized in the presence of CNT (30 wt%) via in-situ polymerization method. 105 The material possesses many advantages to enhance its electrochemical performance. Specifically, the covalent bonding framework improves the stability of the redox-active organic molecules by preventing the redox molecules from dissolving in the electrolyte. In addition, the mesoporous framework facilitates ion transport by providing shortened diffusion pathway between the layers. Lastly, the presence of CNT boosts the overall electrical conductivity of the electrode. Conceptually, the enlisted features make the composite material ideal for Li-ion battery cathodes. However, the proof-of-concept study reported relatively low capacity values, only ~70 mAh g<sup>-1</sup> at 2.4 C. Organic COF anode was first studied by Yang and coworkers using a framework formed between the highly conductive polyporphyrin (TThPP) and 4-thiophenephenyl groups. 112 The COF anode was synthesized via in-situ chemical oxidative polymerization on the surface of copper foil, and exhibited a high reversible capacity of 666 mAh g<sup>-1</sup> at 200 mAh g<sup>-1</sup> and good cycling stability. The excellent electrochemical performance was attributed to the abundant Li adsorption sites as well as the alignment of 2D polyporphyrin sheets leading to the formation of a film on the surface of the copper foil, which can promote the transport of Li-ion and high electronic conductivity over the framework. It should be noted that this COF, like many other COF-based anode materials, stores charge by (de)intercalation mechanism instead of redox reactions.

#### 4.1.1 | Molecular Design

There has been active research for developing new COFs with novel molecular configurations that are dedicated to battery electrode applications. 106,107,113,114 For instance, Yang et al. reported COFs based on 2,7-diaminobenzo[lmn] [3,8]phenanthroline-1,3,6,8(2H,7H)-tetraone (DANT) and two different linker, namely 1,3,5-triformylphloroglucinol (Tp) and 1,3,5-triformylbenzene (Tb). The COF integrated with Tb linker showed superior electrochemical performance in many aspects, including specific capacity, rate-performance, and cycling stability, although the molecular weights of the two linkers are very similar. This study indicates that the enhanced electrochemical performance may be due to the conjugation of the COF backbone that facilitates charge transport and Li-ion diffusion, and possibly microstructure evolution like ligand substitution. The lack of redox-active sites in the framework has always been a critical issue for all COF electrode materials whose charge storage capacity is dominated by the surface redox reaction mechanism. Often in time, only one moiety from the framework could contribute to the charge storage process. However, a recent study from Zhao et al. presented a novel

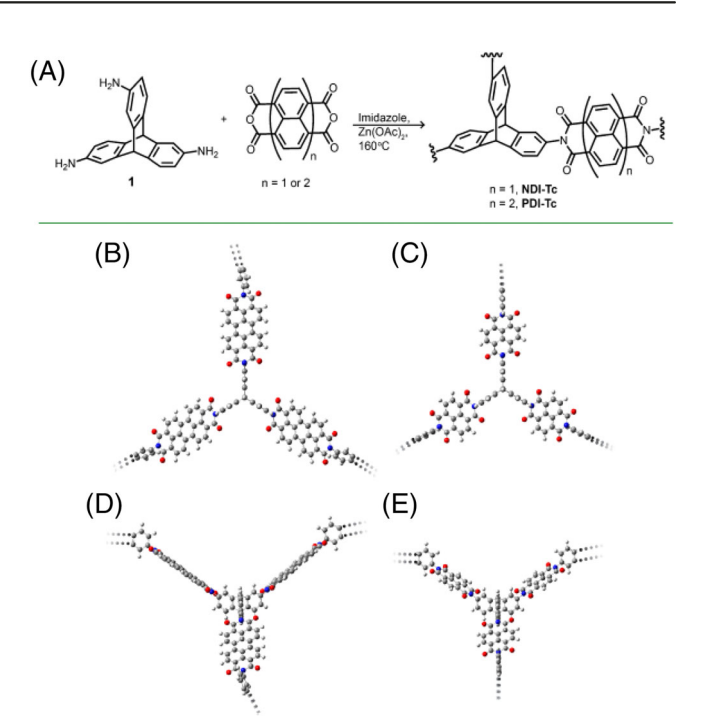
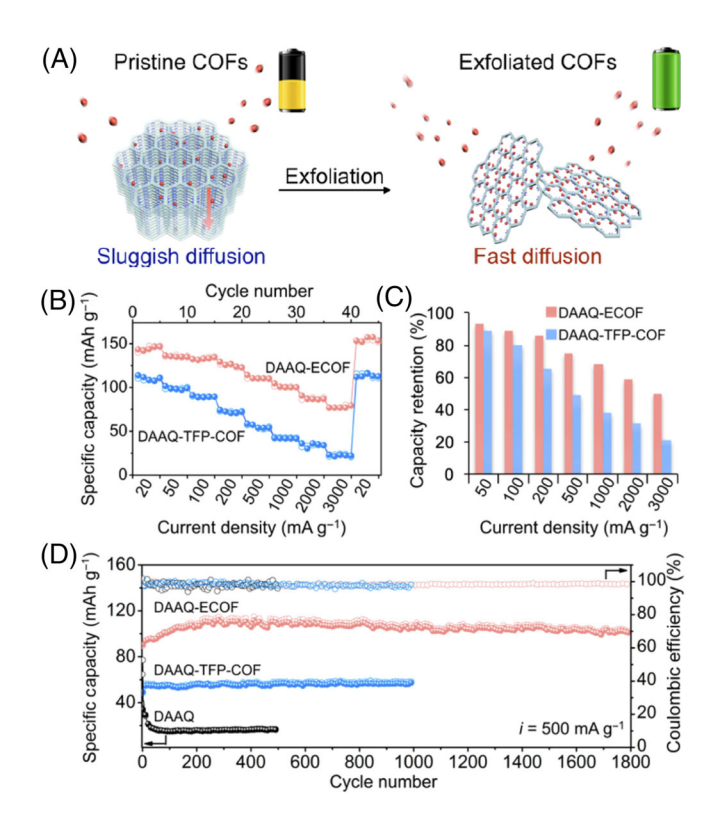


FIGURE 10 (A) Synthesis of PDI-Tc and NDI-Tc 3D frameworks and simulated structure of the (B,D) PDI-Tc repeat unit and (C,E) the NDI-Tc repeat unit calculated using density functional theory. 108 Reproduced with permission: Copyright 2017, American Chemical Society (further permissions related to the material excerpted should be directed to the ACS)

Tp-Azo-COF anode integrated with carbonyl (C=O) and azo (N=N) dual active sites, where the framework could store 30 Li-ions per unit cell.<sup>51</sup> The resulting COF could deliver a reversible capacity of 305.97 mAh g<sup>-1</sup> at a current density of 1 A g<sup>-1</sup> after 3000 cycles thanks to its abundant redox-active sites, large surface area, porous structure, and high stability. The preliminary report of 3D COF electrodes is also noteworthy, as their structural complexity offers various aspects of functional design potentials that hold a great prospect for future energy storage materials. Schon and co-works created a 3D COF based on triptycene and pervlene diimide (PDI), as shown in Figure 10.108 Using the PDI-based redox sites, the cathode exhibited a specific capacity of 75.9 mAh  $g^{-1}$  at a rate of 0.05 C, which is 78.7% of the theoretical value with PDI-Tc, and over 80% capacity retention after 500 cycles. Much more research is still required on the chemical and structural design to realize the true potential of 3D COF-based electrodes.

#### 4.1.2 | Exfoliation of COFs

Exfoliation of 2D COFs from bulk agglomerate to single or few layers has proven to be an effective strategy to improve the electrochemical performance of COF-based



**FIGURE 11** (A) Schematic illustration for the exfoliation of 2D redox-active COFs into exfoliated COFs as cathodes for lithiumion batteries. (B) Rate cyclability and (C) capacity retention of DAAQ-ECOF and DAAQ-TFP-COF compared with their capacities measured at 20 mA g $^{-1}$ . (D) Long-term cyclability and Coulombic efficiencies measured at a current density of 500 mA g $^{-1}$ . (Eproduced with permission: Copyright 2017, American Chemical Society

electrodes. In 2017, Wang et al. reported the exfoliation of COFs into few-layer nanosheets by means of solid-state vibratory ball milling at 50 Hz for 0.5 h.65 The delaminated 2D DAAQ-ECOF nanosheets had ~10-15 atomic layers and exhibited significantly higher discharge capacity compared to their bulk counterpart, particularly at higher rates (Figure 11). At 500 and 3000 mA g<sup>-1</sup>, DAAQ-ECOF gives 107 and 76 mAh g<sup>-1</sup> of discharge capacity compared to ~55 and ~22 mAh g<sup>-1</sup> of the pristine DAAQ-COF. The increased charge storage capacity is mainly due to shortened ion diffusion path enabling significantly better utilization efficiency of the redox sites (~96%) as well as faster kinetics. Its rate-performance and cycling stability were also superior,  $100 \text{ mAh g}^{-1}$  at  $1 \text{ A g}^{-1}$  (more than twice the bulk COF) and no significant capacity loss over 1800 cycles. With further optimization using 1,4-benzoquinone, a redox molecule that has a higher specific capacity, DABQ-ECOF could reach a capacity as high as 210 mAh g<sup>-1</sup> with a voltage plateau of 2.8 V versus Li/Li<sup>+</sup>. The exfoliation process of COF has improved the electrochemical

performance to be considered as a viable and competitive candidate for organic battery electrodes. It is worth noting that ball milling at higher intensity results in reduced capacities over cycling after tens of cycles, rather than leading to better exfoliation effect and electrochemical performance. It is speculated that if the exfoliated nanosheets become thinner, the stability of covalent organic nanosheet (CON) will also decrease, causing partial decomposition of CON. Similarly, the exfoliation approach has proven successful in anode applications. 115-117 Haldar et al. studied the chemical exfoliation methods for COF using maleic anhydride as a functionalizing exfoliation agent. The delamination process simultaneously introduced Li-interacting carbonyl groups. Much improved ion diffusion kinetics and a large number of redox sites (30 Li-ion per unit cell) led to a significantly improved specific capacity of 790 mAh g<sup>-1</sup> compared to that of the pristine COF (200 mAh g<sup>-1</sup>) at 100 mA g<sup>-1</sup>. A full cell using anthracenebased COF anode and LiCoO2 cathode delivered a high specific capacity of 220 mAh g<sup>-1</sup> over 200 cycles. A chemical stripping strategy was also developed by Chen and colleagues to obtain few-layered COF nanosheets (E-TFPB-COF) with embedded MnO<sub>2</sub>. 117 While the exfoliated COF exhibits superior Li-ion storage capability due to enhanced charge diffusion and increased accessible Li storage sites, the embedded MnO<sub>2</sub> nanoparticles can effectively prevent the agglomeration of the exfoliated nanosheets during cycling, thus further improve the long-term stability of the composite electrode. The exfoliated COF anode and its composite with MnO2 exhibited impressive capacities of 968 and 1359 mAh g<sup>-1</sup> at 0.1 A g<sup>-1</sup> versus Li/Li<sup>+</sup>, respectively. An acid-base intercalation mechanism has also been reported for oxidative exfoliation of covalent triazine network, demonstrating enhanced anodic electrochemical performance.116

## 4.1.3 | Composite electrodes with conductive carbon substrates

Hybridization of COFs with nanocarbons (e.g., CNT and graphene) has been a common design strategy in the study of COF as well as other organic electrode materials owing to various advantages of composites, such as improved electrical conductivity, larger specific surface area, better thermal/chemical stability, and strengthened structural integrity. In comparison, the carbon composite electrodes generally outperform the pristine COF, even though a large quantity of conductive carbon is also typically applied in the slurry preparation process. 50,109 Luo et al. developed a poly(imide-benzoquinone) COF via in situ polymerization on graphene (PIBN-G). The synergistic effect from the composite structure allows

for favorable charge transfer properties and full access to redox-active carbonyl groups for both Li-ions and electrons. The composite electrode delivered large reversible specific capacities of 271.0 and 193.1 mAh  $\rm g^{-1}$  at 0.1 and 10 C, respectively, with more than 86% capacity retention after 300 cycles. Wang and coworkers also synthesized polyimide (PI)-based COFs (PI-COFs) and their composite with rGO by simultaneously forming a homogeneous mixture and exfoliated COF nanosheets via ball milling and showed improved electrochemical performance.  $^{109}$ 

There have also been many recent reports of COF battery electrodes that use CNT networks as substrates. Lei and coworkers developed an organic anode consisting of a CNT substrate and a few-layered conjugated COF that has a 14-electron redox chemistry for repeat units. 48 Detailed DFT calculations and electrochemical analysis suggest that the Li-ion storage mechanism corresponds to

redox reactions with six Li-ions per benzene ring as well as typical C=N groups (1 ion per group), which is quite intriguing in the fact that the benzene ring does not exhibit redox activity in its pristine form. The authors ascribed this phenomenon to the effect of COF@CNT structure that enables the controlled synthesis of fewlayered COF in the CNT network. This structure is more favorable for Li-ion insertion into the interlamination of the 2D lamellar structure compared to the pristine COF anode and can promote the redox reaction in more functional units. Due to the activation of the additional redox-active sites in benzene rings, the COF@CNT anode delivered a high reversible capacity of 1536 mAh g<sup>-1</sup> and stable cycling performance over 500 cycles. A similar design approach has also proven successful in cathode design. Yao et al. developed a boroxine-linked chemically active pyrene-4,5,9,10-tetraone (PTO) COF (2D PPTODB

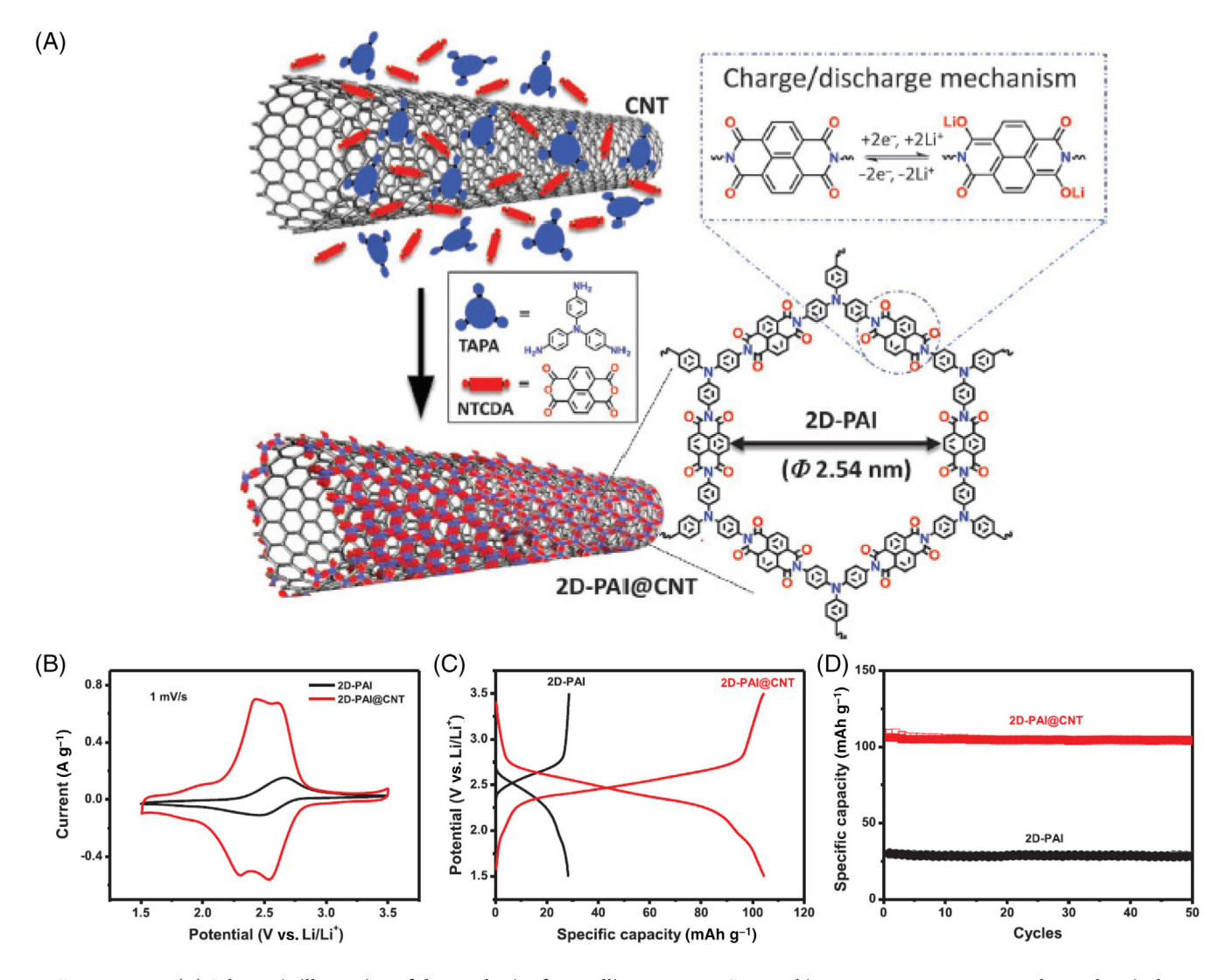


FIGURE 12 (A) Schematic illustration of the synthesis of crystalline 2D-PAI@CNT and its energy storage process. Electrochemical performance of 2D-PAI and 2D-PAI@CNT. (B) CV curves at 1 mV s $^{-1}$ , (C) galvanostatic charge–discharge curves, (D) cycling performance of 2D-PAI and 2D-PAI@CNT at 0.1 A g $^{-1}$ . <sup>110</sup> Reproduced with permission: Copyright 2019, John Wiley and Sons

COFs). The binder-free cathode with 70 wt% PPTOBD COF and 30 wt% CNT delivered a high specific capacity of 198 mAh g<sup>-1</sup> with fair rate-capability. Increasing the proportion of CNT can further improve the charge-storage performance of the organic electrode by faster kinetics and more efficient utilization of redox-active sites. Wang et al. demonstrated that the composite 2D-PAI@CNT cathode (PAI:CNT 1:1) showed little capacity loss between 0.2 and 2 A g<sup>-1</sup> and achieved 100% capacity retention over 8000 cycles (Figure 12).<sup>110</sup>

#### 4.2 | Sodium-ion batteries

Important findings in COFs also have been made over the studies of COF redox reactions with sodium (Na)ions. 49,57,118-120 Liu and colleagues reported a crystalline 2D conjugated polymer via C-C coupling reaction in 2017.<sup>57</sup> Prior to this study, COF linkages typically involve imine and phenazines, and the construction of crystalline organic structure using stronger covalent bonds such as C—C bonds was not realized because the irreversible C—C formation prevents self-correction during the growth of organic framework. The remaining defects consequently reduce the crystallinity of the material. To overcome this obstacle, the authors designed a precursor, 2-TBQP (2,7,13,18-tetrabromodibenzo[a,c] dibenzo [5,6:7,8]quinoxalino-[2,3-i]phenazine), from which a crystalline 2D-conjugated aromatic polymer (2D-CAP) can be constructed by C—C coupling of the monomers in the crystalline state by preordering the monomers prior to endogenous solid-state polymerization that minimizes the defects induced in the framework. The synthesized crystal had a layered stacking structure with highly ordered 1D channels and can be easily exfoliated into nanosheets. When the exfoliated 2D-CAP was employed as the organic anode for Na-ion batteries, the electrode containing a small amount of carbon additive (10 wt%) delivered a stable reversible capacity of 105 mAh g<sup>-1</sup> at a high current rate of 10 A g<sup>-1</sup> as well as exceptional cycle stability over 7500 cycles. The enhanced chemical stability and conductivity provided by crystalline organic polymers with C—C bonding hold great potential to overcome the weaknesses of traditional COFs. According to another report on the CON sodium-ion anode by Kim et al., a similar effect on improving electronic/ionic conductivity can also be achieved by adopting monomers with high polymer backbone planarity and specific surface area. 119

Many organic redox materials turn into radical intermediate states during the process of charge and discharge. While high radical reactivity is favorable to full utilization of accessible ion storage sites, the possibility of side reactions with other active molecules would also lead to irreversible capacity loss of the electrode. The stability of COF radical intermediates and their dependence on COF thickness was systematically studied by Gu and colleagues. 118 Choosing the conventional β-ketoenamine linked COFs as the subject, the comprehensive spectroscopic analysis indicated that the COFs undergo radical formation and transformation during the redox reactions, and that stacking thickness is a crucial factor for the electrochemical performance of the intermediates. Aside from other known benefits such as higher surface area, more active sites, faster ion diffusion, etc., reducing the stacking thickness of the COFs from the bulk thickness is also beneficial for stabilizing the radical intermediates and maintaining the capacity contribution. The 4-12 nm COF anode delivered high capacities of 420 mAh g<sup>-1</sup> at  $0.1 \text{ A g}^{-1}$  and  $198 \text{ mAh g}^{-1}$  at a high rate of  $5 \text{ A g}^{-1}$  as well as excellent capacity retention over 99% after 10 000 cycles. In comparison, the optimized few-layered COF achieved more than twice the capacity compared to the 100-250 nm thick bulk COF electrode, further validating and rationalizing the importance of COF exfoliation in EES applications.

A recent report by Shi et al. introduced a nitrogen-rich COF (TQBQ-COF) with multiple carbonyl groups that delivered an ultra-high specific capacity of 452 mAh g<sup>-1</sup> as a Na-ion battery cathode (Figure 13).<sup>49</sup> The COF was synthesized via a triple condensation reaction between tetraminophenone (TABO) and cyclohexanehexaone (CHHO). Spectroscopic analysis and DFT calculations uncovered that both pyrazine (C=N) and carbonyl (C=O) groups undergo redox reactions, and each COF unit could store up to 12 sodium-ions collectively. Replacing the inactive linker molecule with both redox-active constituents greatly improved the capacity contribution from the COF electrode. Additionally, the introduction of nitrogen reduced the energy gap between the lowest unoccupied molecular orbital (LUMO) and the highest occupied molecular orbital (HOMO), thus allowing the COF to possess high electronic conductivity (~10<sup>-9</sup> S cm<sup>-1</sup>) and ionic conductivity (~10<sup>-4</sup> S cm<sup>-1</sup>), further elevating its rate-performance. The level of performance achieved by building blocks that are both redox-active represents great potential for the practical applications of COFs as energy storage materials.

#### 4.3 | Potassium-ion batteries

Recently, potassium (K)-ion batteries (PIBs) have been proposed as a new energy storage system due to the abundant potassium resources and low electrolyte costs. However, the formation of dendrites by active K-ions on the anode poses a serious hazard in cell cycling.

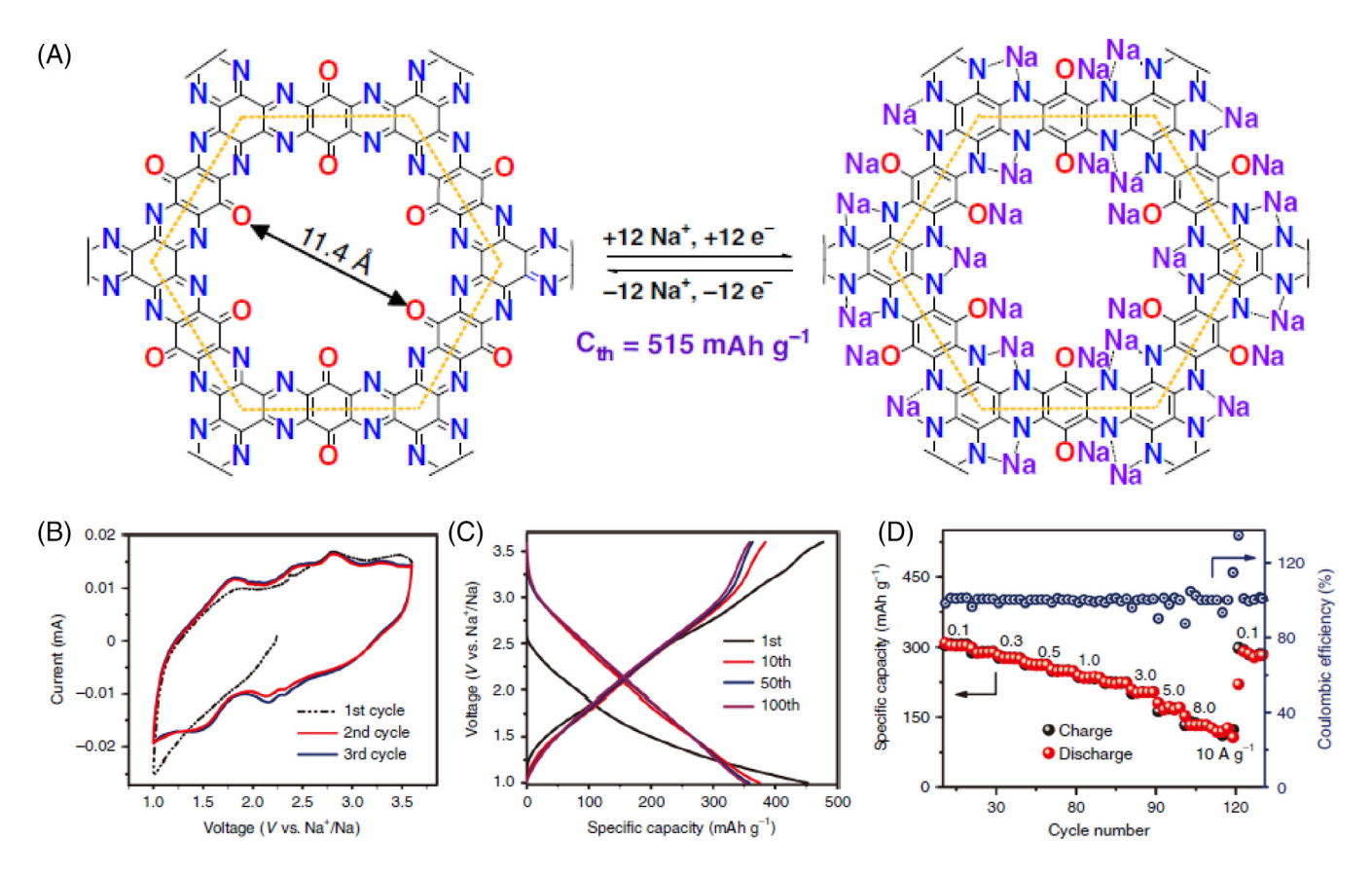


**FIGURE 13** (A) The chemical structure and possible electrochemical redox mechanism of TQBQ-COF with a theoretical capacity of 515 mAh  $\rm g^{-1}$ . (B) CV curves of the TQBQ-COF electrode at a scan rate of 0.2 mV s<sup>-1</sup>. (C) Charge–discharge profiles of the TQBQ-COF electrode at 0.02 A  $\rm g^{-1}$ . (D) The rate performance of the TQBQ-COF electrode from the current density of 0.1–10 A  $\rm g^{-1}$ , then back to 0.1 A  $\rm g^{-1}$ . (P) Reproduced with permission: Copyright 2020, Springer Nature

Therefore, it is important to develop novel materials that suppress the formation of dendrites. Compared to inorganic materials, organic electrodes are low-cost and environmentally friendly. Although most organic materials suffer from several issues such as low electronic conductivity, dissolution in the organic electrolyte, and low reversible capacities, the advances in 2D COF material could largely mitigate these shortcomings. 121-123 A fewlayered boronic ester-based COF was synthesized by Chen et al. via in situ growth on CNT and examined as the anode material for PIB. 121 The hierarchical porous structure formed between CNT and few-layered COF facilitates the transport of K-ions and provides sufficient void space to effectively buffer volume changes during the potassisation/depotassisation process. When the CNT network effectively reduces the electrical resistance, the few-layered COF-10 also provides exposure to more active site exposure and shorter charge diffusion pathways. Therefore, both the insertion/extraction kinetics of K-ions and the charge storage capacity of the electrode were significantly improved. Thus, the COF-10@CNT anode exhibited a high reversible capacity of 288 mAh g<sup>-1</sup> after 500 cycles at 0.1 A g<sup>-1</sup>. Additionally,

the porous structure also offered buffer space for volume changes during potassisation/depotassisation process and stabilized the battery system, which was able to maintain a reversible capacity of 161 mAh  $\rm g^{-1}$  after 4000 cycles at 1 A  $\rm g^{-1}$ .

#### 4.4 | Lithium-sulfur battery

Besides transitional metal-ion batteries, COFs have found great prospects in lithium (Li)-sulfur (S) batteries. Li-S batteries have attracted much attention due to their superior theoretical capacity (1672 mAh g<sup>-1</sup>) and specific energy density (2600 Wh/kg) compared to state-of-the-art LIBs. However, despite their great potential, the Li-S batteries suffer from several critical flaws in the application, most significantly the "shuttle" effect, where intermediate polysulfide species tend to diffuse into the electrolyte solution and migrate between cathode and anode. The "shuttle" phenomenon results in a reduced practical capacity, active mass loss, and poor cycle stability. One of the most effective strategies to suppress the shuttle effect is to construct the cathode with a partially

enclosed surface morphology that constrains sulfur and polysulfide species within confined space, thus maintaining the structural integrity and composition of the electrode. The optimal host material for sulfur should be lightweight, conductive, and have a stable porous structure with a high surface area. Owing to their well-defined nanoporous structure and exceptional mechanical and chemical stability, 2D COFs are considered to be ideal candidates for sulfur/polysulfide host material in principle and have shown great promises in recent studies.

The impregnation of sulfur into COFs was first demonstrated by Liao and coworkers in 2014, where a semiconducting 2D COF, CTF-1, was used as the sulfur host material using a melt-diffusion strategy. CTF-1 and sulfur were mixed at room temperature and heated at 155°C for 15 h to allow sufficient sulfur diffusion into the CTF-1 nanopores (Figure 14A). The process of sulfur diffusion was verified by the differences shown in PXRD as well as specific surface area, which was reduced due to sulfur clots in the nanochannels. The electrochemical performance of the CTF-1/S electrode showed good rate

performance and short-term cycling stability within 50 cycles, particularly at an elevated temperature of  $155^{\circ}\text{C}$  (Figure 14B–D). In a subsequent study, the authors also investigated porphyrin-based COFs for sulfur storage.  $^{126}$  With relatively high charge carrier mobility and larger pore dimensions compared to other organic crystalline conductive polymers, the Por-COF/S cathode delivered 633 mAh g $^{-1}$  at 0.5 C after 200 cycles under room temperature with a decay rate of 0.16% per cycle.

As with the redox metal-ion electrode, the COF-sulfur cathode offers lots of potential for chemical and mechanical tuning to optimize the interaction between the polysulfide species and the host material. For instance, Ghazi et al. suggested the use of boronate ester COFs as a sulfur host to enhance the chemisorption of LiPS (lithium polysulfide). While the N-doped linkages only absorb Liions, the dense and uniform distribution of positively polarized B and negatively polarized O atoms on the linkages guarantee simultaneous adsorption of  $S_x^{2-}$  and Liion in soluble LiPSs and thus render sulfur redeposition more uniform. Comparing the electrochemical performance of the sulfur cathodes stored in COF-1 and CTF-1

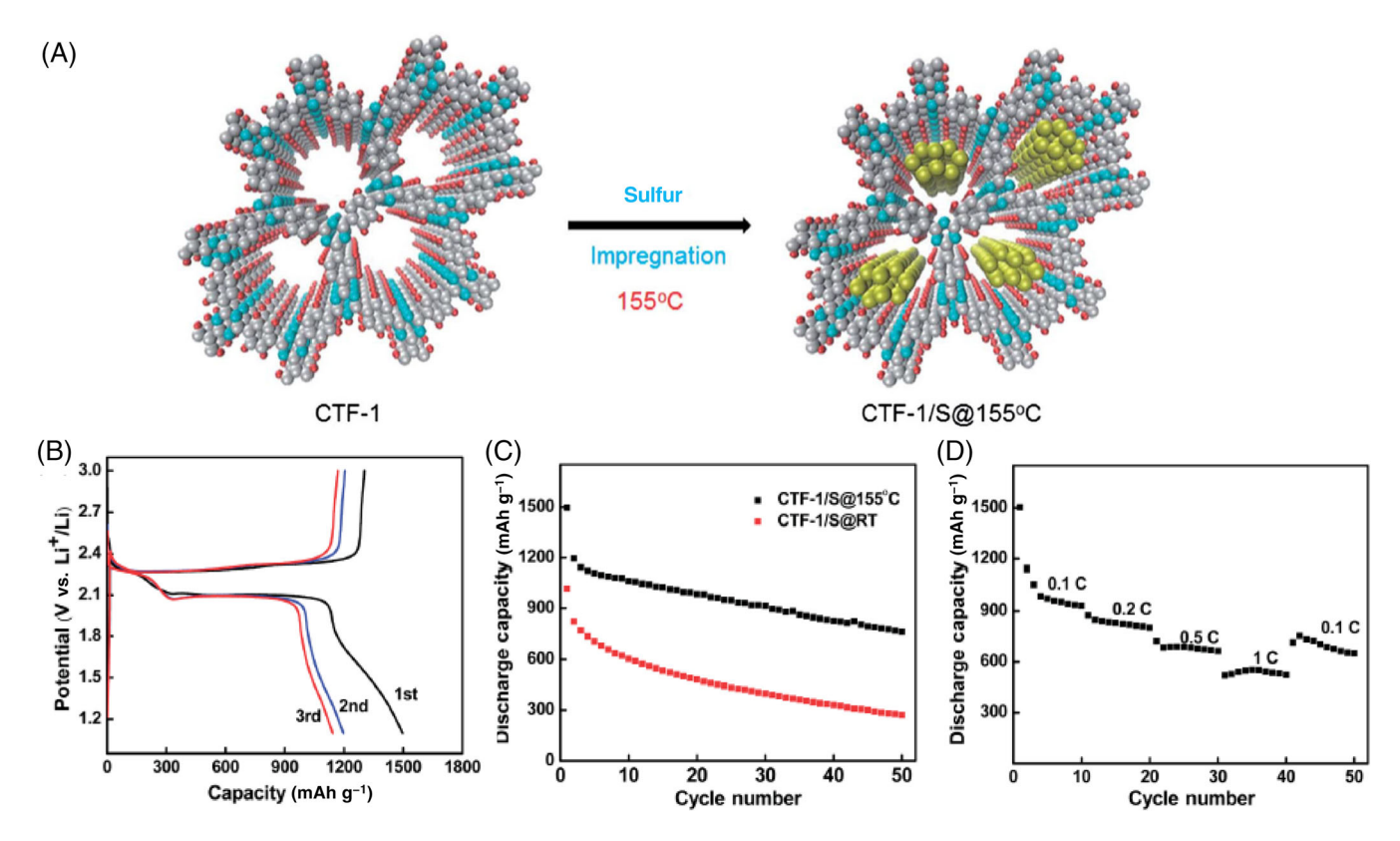


FIGURE 14 (A) Schematic diagram of the composite synthesis from CTF-1 by impregnation of molten sulfur. The carbon is shown in gray, the nitrogen in blue, the hydrogen in red, and the sulfur in yellow. (B) Galvanostatic discharge and charge profiles of the CTF-1/S@155 C composite at a 0.1 C rate; (C) cycling performance of CTF-1/S@155 C and CTF-1/S@RT at a 0.1 C rate; (D) discharge capacity for the CTF-1/S@155 C composite at different rates. The voltage range used was between 1.1 and 3.0 V versus Li and the electrolyte was 1 M lithium bis(trifluoromethane sulfonyl)imide in dimethoxyethane and 1,3-dioxolane (1:1, v/v). Reproduced with permission: Copyright 2014, Royal Society of Chemistry

with similar pore sizes, COF-1/S showed better cycling performance, delivering 929 mAh g<sup>-1</sup> after 100 cycles at 0.2 C compared to 489 mAh g<sup>-1</sup> from CTF-1/S. The difference was attributed to the positively polarized surface in COF-1 caused by the electron-deficient B atoms, which can trap the negatively charged polysulfides. The superior sulfur storage capacity of COF-1 was also supported by optical examination, XPS as well as DFT calculations, indicating that the binding energies between the  $S_x$  moieties and the layered COF-1 were found to be significantly lower than that of the CTF-1, hence much stronger PS absorption. Fluorinated CTF was also shown to further improve sulfur storage performance by accelerating polysulfide conversion and further enhanced the binding interaction. 128 Subsequent studies on this subject also employed pyrene-based COFs and hybrid COFs containing triazine and boroxine units with better

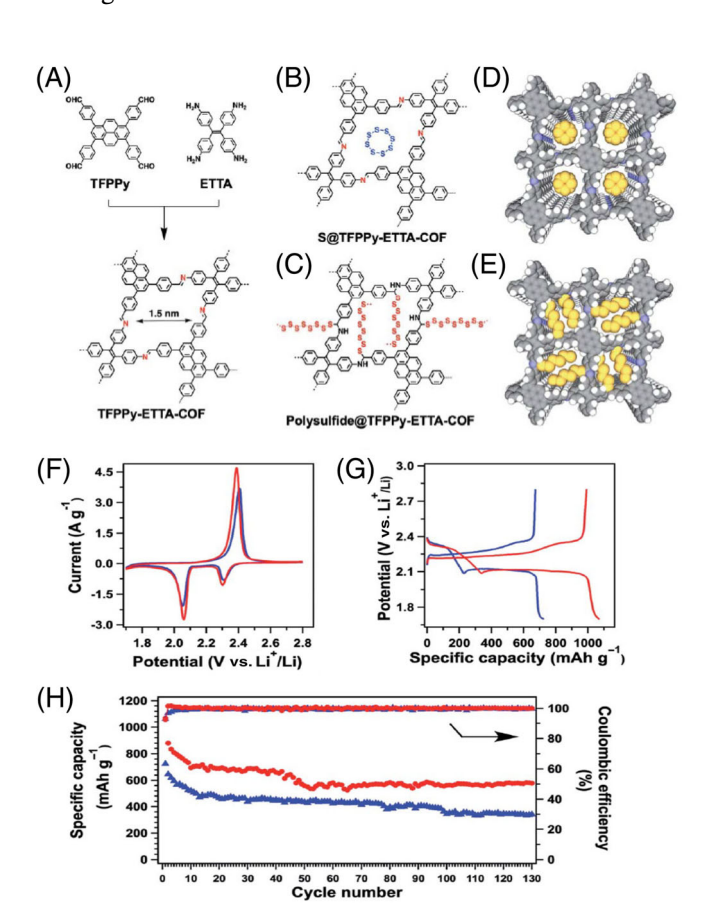


FIGURE 15 (A) Schematic of the synthesis of TFPPy-ETTA-COF. (B) Physical isolation of sulfur (S8 ring) in the COF. (C) Covalent engineering of polysulfide chains on the pore walls. (D) Graphic of sulfur loaded in S@TFPPy-ETTA-COF. (E) Graphic of polysulfide chains locked in polysulfide@TFPPy-ETTA-COF. (F) Electrochemical performance of S@TFPPy-ETTA-COF (blue) and polysulfide@TFPPy-ETTA-COF (red). (F) CV profiles at a scan rate of 0.1 mV s<sup>-1</sup>. (G) Charge–discharge profiles at 0.1 C. (H) Cycling performances and Coulombic efficiency. <sup>131</sup> Reproduced with permission: Copyright 2019, Royal Society of Chemistry

polarization characteristics to further optimize sulfur storage conditions.  $^{54,129}$  In particular, the binary TB-COF with both triazine and boroxine linages enabled cooperative trapping of LiPSs through the lithiophilic and sulfiphilic interactions, delivering an impressive reversible capacity of  $663 \text{ mAh g}^{-1}$  after 800 cycles at 1 C and highlighting the potential for the rational design of bifunctional COFs.

Aside from molecular design, studies have also been conducted to adjust the macro/microstructures beyond the pore dimensions to improve sulfur storage. For instance, Yoo et al. proposed a self-standing COF-CNT net hybrid architecture with hierarchical pores as a chemical trap for lithium polysulfide. 130 The COF-net on CNT-net (NN) interlayers were fabricated through CNTtemplated in-situ COF synthesis and inserted between the sulfur cathode and the separator. The effects of pore size and chemical affinity were also studied by comparing COF-1(0.7 nm) and COF-5 (2.7 nm). Benefiting from the hierarchically porous structure and strong chemical absorption, the interlayers effectively captured Li<sub>2</sub>S<sub>x</sub> without impairing charge conduction. In particular, the tailored microstructure and high chemical affinity of COF-1 NN interlayer enabled selective deposition/dissolution, which provides a significant improvement on the electrochemical performance of the Li-S battery system, delivering 84% capacity retention after 300 cycles at 2 C compared to 15% of the pristine cell. Xu et al. also discovered that the imine linkages in COF can trigger the polymerization of sulfur into polysulfide chains at high temperatures, hence suppressing the shuttle effect via the covalent C-S bond (Figure 15). 131 Polymerized polysulfide is not only much more stable than elemental sulfur in the electrode, but also facilitates the redox kinetics as well as charge conductance and transport.

#### 4.5 | Charge conduction in COFs

Despite the high charge-carrier mobility in COFs, their low intrinsic electrical conductivity poses a great challenge to many applications in EES. Along with the advances in developing the synthesis process and exploiting the charge storage capabilities, substantial research efforts have been devoted to investigating the charge transport properties and enhancing the conductivity of COF materials to explore the potential as a material platform for other battery cell components such as solid electrolyte and separator. Effective strategies reported for promoting ionic conduction in COF include alignment of ionic transport pathways, 132,133 the use of ionic framework, 134,135 and doping of conducting additives. The correlation between ionic conductivity and crystallographic alignment of COF

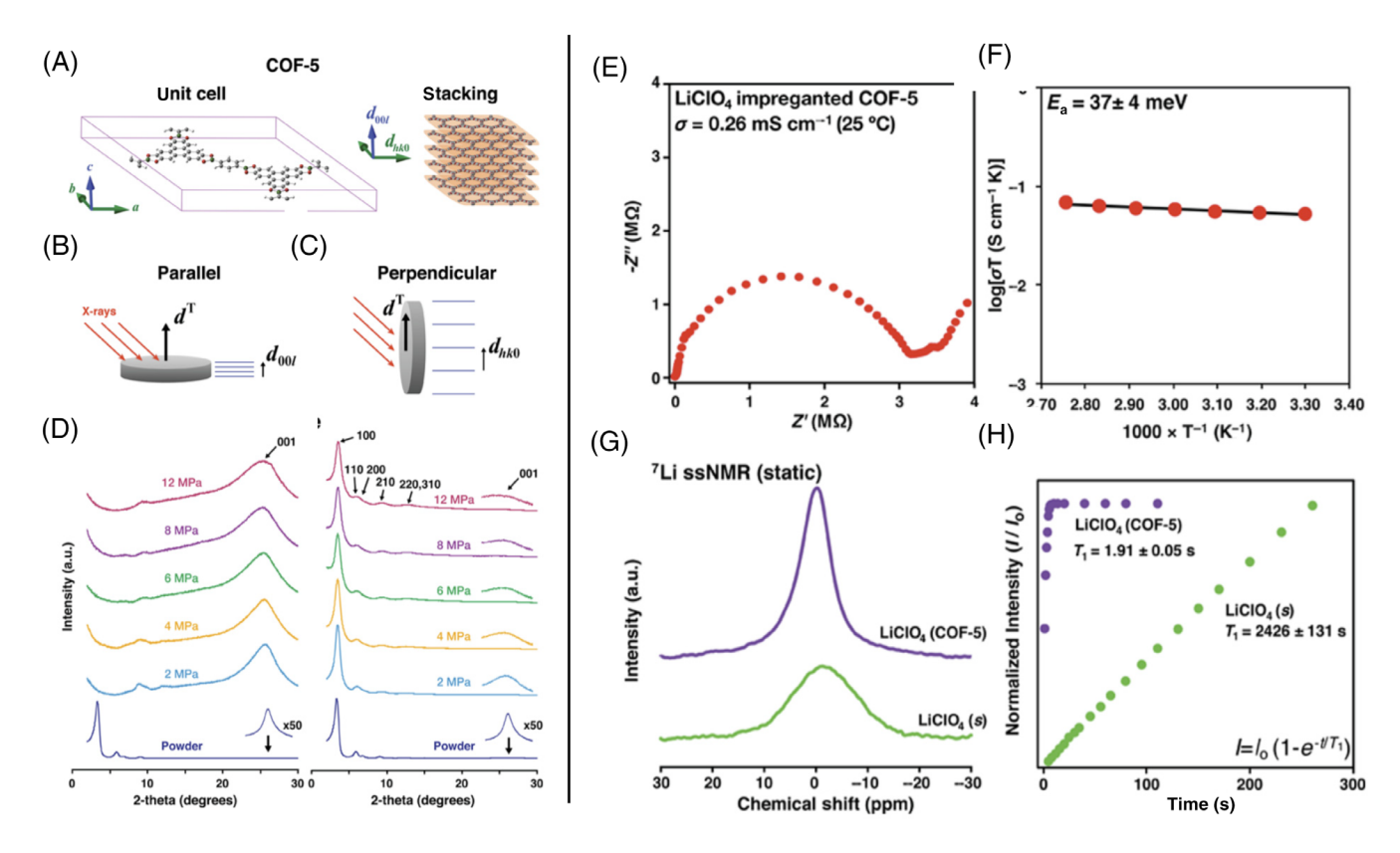
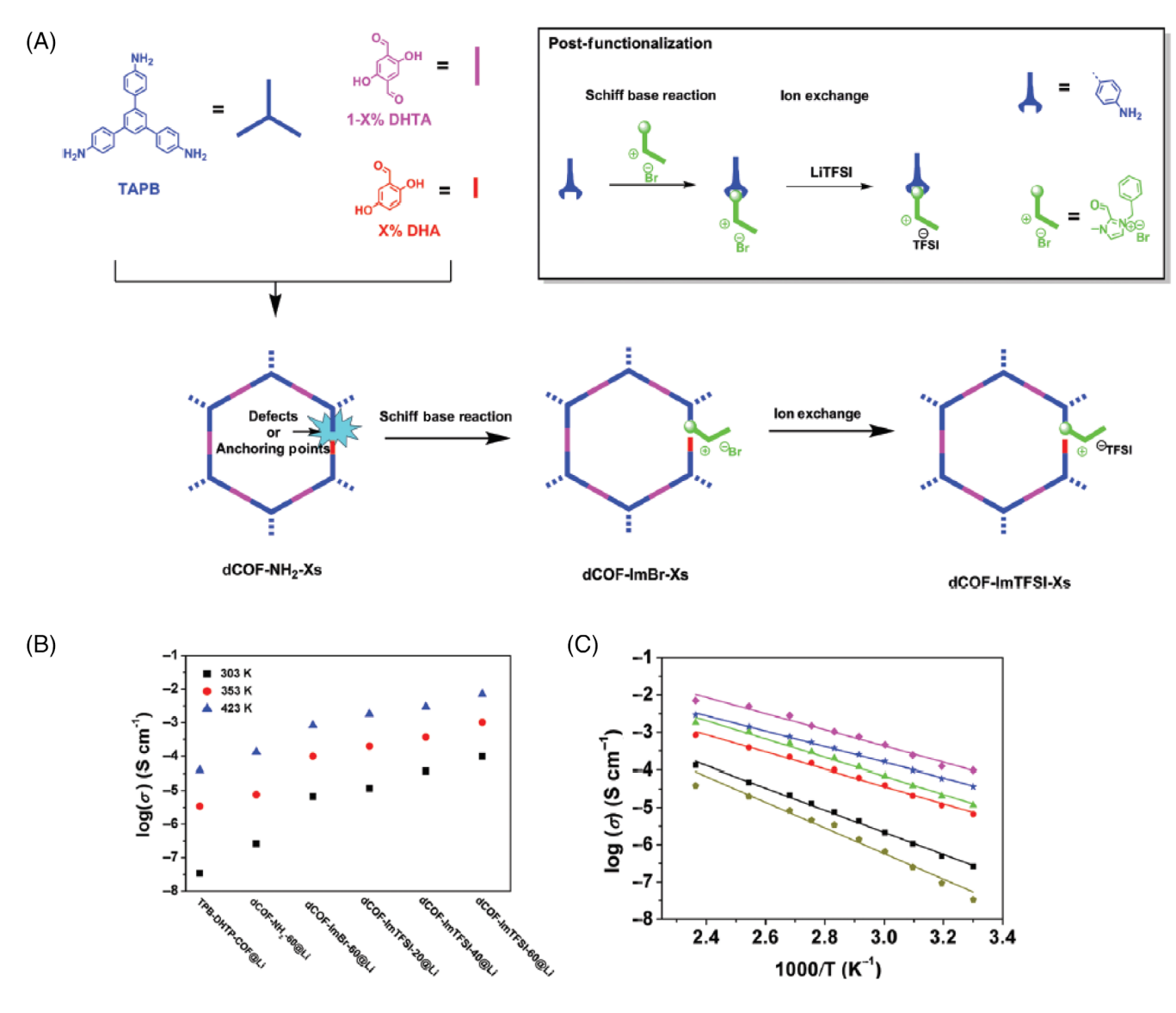


FIGURE 16 (A) Unit cell of COF-5 illustrating the stacking and orthogonality between dhk0 and d00l plane normal vectors. (B) COF pellet oriented parallel to the optical axis and (C) corresponding PXRD of COF-5. (D) COF pellet oriented perpendicular to the optical axis and (E) corresponding PXRD of the COF-5 pellet. (E) Complex impedance function and (F) Arrhenius plot of COF-5 impregnated with LiClO4; (G) Static 7Li ssNMR spectra and (H) saturation recovery plot of COF-5 impregnated with LiClO4 (purple), compared to pure LiClO4 (green). <sup>132</sup> Reproduced with permission: Copyright 2016, American Chemical Society

was demonstrated by Vazquez-Molina and coworkers. In the study, different COFs were mechanically pressed into pellets with a uniaxial load, and exhibited a similar anisotropic ordering with preferred orientation between hk0 and 00l crystallographic planes (Figure 16). 132 Increased loading in the parallel and perpendicular direction induces greater crystalline strain due to the deviation in the interplanar distance between the layers, which could be relieved after grinding. The morphology of COF also changed from globular agglomerates of COF crystallites in powder form to anisotropic sheet-like formation in pellet form. The pressure-induced crystallographic orientation was observed in other 2D materials via van der Waals interactions, but only at higher pressure. 139,140 This phenomenon is particularly preferred for COFs because they enable alignment of the pore arrangement that can dramatically improve the charge carrier transport. The COF-5 pellet impregnated with LiClO<sub>4</sub> was tested as a solid electrolyte and delivered electric conductivity up to 0.26 mS cm<sup>-1</sup> and good electrochemical stability, while the COF-5 pellet immersed in 1 M LiClO<sub>4</sub>/THF electrolyte solution did not exhibit any Nyquist behavior and tended to lose its

structural integrity. Chen et al. have demonstrated the incorporation of the cationic moieties in the skeleton of COF material that can split the ion pair of Li salts, boosting the concentration of free mobile Li-ions and improving ion conductivity.<sup>134</sup> The covalent organic nanosheets with chloride counterions were synthesized and ionexchanged with LiTFSI, where Cl<sup>-</sup> anions were replaced by TFSI<sup>-</sup> to form CON-TFSI, and lastly mixed with LiTFSI salt. The ionic framework is beneficial for screening Coulombic interactions due to its greater polarizability compared to the neutral framework. The cationic COF exhibited enhanced conductivity up to  $2.09 \times 10^{-4} \, \mathrm{S \, cm}^{-1}$ at 70°C. Under the same principle, Li and coworkers synthesized 2D COFs with varying degrees of defects via a three-component condensation strategy (Figure 17). 135 Imidazolium functional groups were introduced onto pore walls of the COF via Schiff-base reaction and then replaced by TFSI-ions via ion exchange. While maintaining good crystallinity, the COF (dCOF-ImTFSI-Xs) possessed a preferable porous structure with defects to facilitate ion transport. The framework also contained cationic imidazolium moieties and TFSI-anions to promote Li-ion conductance.



**FIGURE 17** (A) Synthesis of dCOF-NH2-Xs by three-component condensation; synthesis of dCOF-ImBr by Schiff-base reaction; synthesis of dCOF-ImTFSI via ion exchange method. (B) Nyquist plots of dCOFs based electrolytes. (C) Arrhenius plot of lithium-ion conductivity of dCOF-based electrolytes. <sup>135</sup> Reproduced with permission: Copyright 2020, John Wiley and Sons

At an elevated temperature of 423 K, the Li<sup>+</sup> ionic conductivity of COF-ImTFSI-60@Li electrolyte was as high as  $7.05 \times 10^{-3} \, \mathrm{S \ cm^{-1}}$ .

The solid-state single Li-ion conduction behavior of COF was investigated by Jeong and colleagues, where a lithium sulfonated COF (TpPa-SO<sub>3</sub>Li) was synthesized and demonstrated as a solvent-free, single Li-ion conductor. The sulfonated COF was rationally designed to possess axially stacked directional ion channels, small pores with a high density of Li-ions and covalently tethered anion groups (Figure 18). It exhibited an ionic conductivity of  $2.7 \times 10^{-5}$  S cm<sup>-1</sup> with a Li-ion transference number of 0.9 at room temperature and an activation energy of 0.18 eV without supplemental incorporation of Li salts or organic solvents. Xu et al. also reported the

synthesis of polyelectrolyte COFs by integrating oligo(ethylene oxide) chains onto the channel wall.  $^{137}$  Upon complexation with Li-ions, the covalent integration of ethylene oxide chains formed a polyelectrolyte interface in the channel, facilitating the dissociation of ionic bonds and offering a pathway for ionic transport between neighboring chains through a vehicle mechanism that reduces the energy barrier. COF with polyelectrolyte interface exhibited ionic conductivities of 6.04  $\times$  10 $^{-6}$ , 2.85  $\times$  10 $^{-5}$ , and 1.66  $\times$  10 $^{-4}$  S cm $^{-1}$  at 40, 60, and 80°C, respectively, which are 44, 42, and 30 times higher than the ionic conductivities of the bare-walled COF without ethylene oxide chains. Lastly, Wen and colleagues also demonstrated a COF-coated Li-ion battery separator.  $^{141}$  The separator was fabricated by coating a custom-



Porous crystalline ion conductors containing Li salt (left) and/or solvent (right)

# This study Covalently tethered anion ... Mobile Li-ion

Solvent-free, single Li-ion conducting COF

FIGURE 18 (A) Conceptual illustrations of ion transport phenomena in the porous crystalline ion conductors. (B) Chemical structure of lithium sulfonated COF (TpPa-SO3Li). Reproduced with permission: Copyright 2019, American Chemical Society

designed COF from 1,3,5-tris(4-aminophenyl) benzene and 2,5-dimethoxybenzene-1,4-dialdehyde on a commercial polymer separator. The COF contained electron-withdrawing methoxy groups with localized negative charges to promote Li-ion transport and polar (—C=N—) groups that could raise Li-ion transference number by suppressing conduction of other undesirable transition metal ions. Therefore, the COF-coated separator can

effectively regulate ion conduction, double the Li-ion transference number, and significantly enhance the cycling stability and rate performance of LIBs.

## 5 | MODELING AND SIMULATIONS

First-principles approach, namely Density Functional Theory (DFT), has been playing a critical role in understanding fundamental mechanisms of electrochemical processes in novel organic electrode materials by investigating the electronic structures and properties. 130,142 In particular, DFT studies can provide valuable insight into charge storage mechanisms, including the intercalation and conversion reactions, and structural evolution of various batteries during operation. 143-149 Therefore. DFT computations can complement and guide experimentation by unveiling the structure-property relationships for a wide range of promising materials, especially focusing on the effect of the chemical structure of COF on electrochemical characteristics. Another powerful simulation method is molecular dynamics (MD) simulation to investigate large-scale structures of COF. 48,150,151 For instance, MD simulation can predict accurate COF structures whose simulated PXRD patterns can be analyzed in conjunction with experimentally observed patterns to investigate a particular stacking arrangement in COF systems. 65,130,152-155 It has been well known that the stacking arrangement is a critical factor that can impact ion mobility and electronic conductivity in COFs. 46,118 However, it should be noted that the results obtained from computational modeling methods are often sensitive to the level of theory employed in characterizing the properties of COF. 156-158 Therefore, selecting appropriate theory and computational conditions is a necessary prerequisite to elucidate target properties successfully.

#### 5.1 | Alkali metal-ion batteries

Computational techniques can help provide detailed information on the association of alkali metal ions with COF and the corresponding structural changes. For instance, Shi et al.<sup>49</sup> optimized the structure of triquinoxalinylene-benzoquinone based COF (TQBQ-COF) using the B3LYP<sup>159</sup> functional with the 6-31G (d) basis set<sup>160</sup> and evaluated its single point energy using B3LYP/6-31G+(d,p) with SMD solvation model.<sup>161</sup> By analyzing the molecular electrostatic potential (MESP), six initial binding sites for Na-ions were determined, and by analyzing the LUMOs, it was revealed that both nitrogen and oxygen contributed to LUMO equally, implying

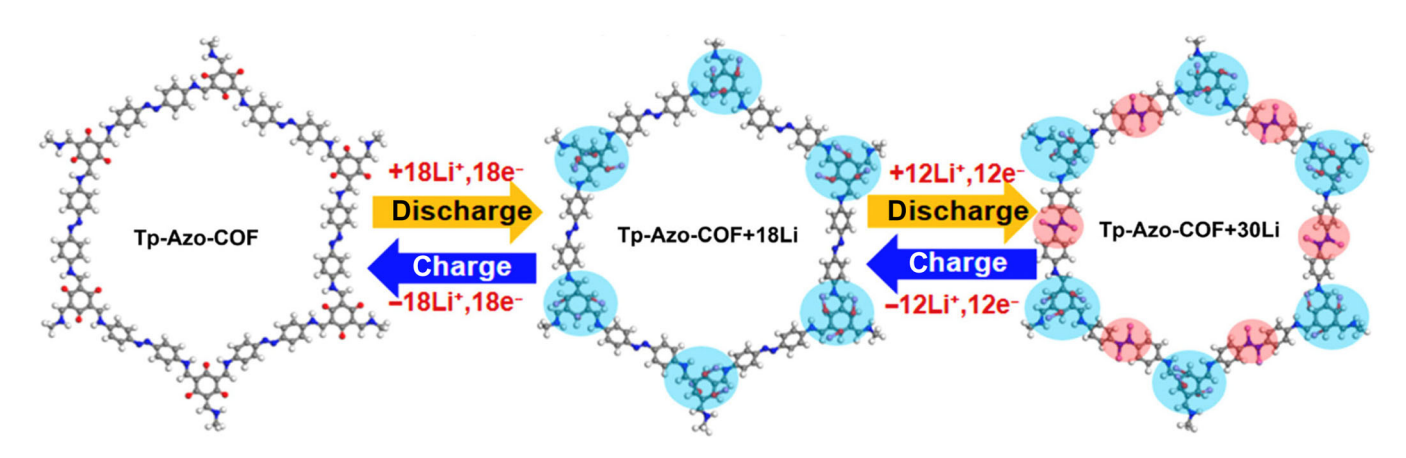


FIGURE 19 Structural evolution of *Tp-Azo-COF* during charging/discharging process. Blue and red spheres represent the binding sites between Li and the C=O and N=N groups, respectively. As depicted, Li preferentially binds first with the carbonyl oxygens for Tp-Azo-COF + 18Li, followed by azo active sites to achieve Tp-Azo-COF + 30Li.<sup>51</sup> Reproduced with permission: Copyright 2020, American Chemical Society

that N and O can stabilize Na-ions cooperatively. Indeed, this computational finding was experimentally confirmed through FTIR and XPS, exhibiting that the intensities of C=N and C=O groups are weakened simultaneously as a function of binding during the discharging process.<sup>49</sup> Further MESP computation for Na<sub>6</sub>-TOBO-COF discovered six additional binding sites for Na-ions, and thereafter no additional binding sites were discovered for Na-ions in Na<sub>12</sub>-TOBO-COF. Therefore, it was concluded from DFT calculations that each TQBQ-COF unit can accommodate up to 12 Na-ions. It was also found that the average potentials for Na<sub>6</sub>-TQBQ-COF and Na<sub>12</sub>-TQBQ-COF were 2.79 and 1.59 V, respectively, 49 indicating that the potential is reduced as a function of the number of Na-ions accommodated in TOBO-COF. On the other hand, Wu and co-workers proposed to utilize TQBQ-COF for LIB, 162 in which the most optimal configurations for Li-ion binding were determined using DFT calculations with B3LYP/6-31G+(d,p). As reported for Na-ions, 49 up to 12 Li-ions can be accommodated in TOBO-COF through association with the oxygen atoms of carbonyl (C=O) groups and the nitrogen atoms of the imine (C=N) groups. 162 It was found from DFT calculations that the Li-ion binding energy is drastically destabilized beyond 12 Li-ions associated in TQBQ-COF, which was also confirmed experimentally. 162

Since the high theoretical capacity of TQBQ-COF with respect to Na- and Li- ions can be attributed to its many redox-active groups, it is not surprising that enhancing the number of available binding sites for alkali metal ions is critical for designing high-capacity electrodes. To maximize the electrochemical redox activity, a novel 4,4'-azodianiline (Azo)-1,3,5-triformylphloroglucinol (Tp) based COF (Tp-Azo-COF) with active C=O and N=N (azo) active sites

through  $\beta$ -ketoenamine linkage has been synthesized and applied for LIBs. <sup>51</sup> As shown in Figure 19, DFT calculations exhibit that this proposed COF can theoretically accommodate up to 30 Li-ions through binding with C=O sites first and then N=N sites. <sup>51</sup>

Recently, three azo-based COF structures were examined by Singh and colleagues. 163 In addition to the Tp-Azo-COF with β-ketoenamine linkage, thiazole and imine-based linkages were also investigated. Compared to the thiazole-linked COF (Figure 20A) exhibiting an extended  $\pi$ -conjugation and high stability, the azo-based COFs with the imine and β-ketoenamine linkages undergo a much more rapid degradation. The superior electrochemical performance of the thiazole-linked COF is further attributed to its fast two-electron transfer process in one step for both cathodic and anodic responses, which is contrasted with imine-based COF preferring a stepwise electron transfer. DFT calculations confirmed this phenomenon by showing that the reduction potentials corresponding to the first and second Li-ion association to the azo group in single layer thiazole COF were 2.05 and 1.97 V, respectively. Since the difference between the potentials (2.05 and 1.97 V) is within the range of DFT uncertainty, such a negligible potential drop indicates that a fast two-electron transfer process is favorable, which leads to the simultaneous association of two Li-ions to the azo groups in the thiazole-linked COF. 163 Although β-ketoenamine COF would have higher conductivity due to its smaller band gap (0.17 eV) compared to thiazole- and imine-based COF (1.46 and 1.29 eV, respectively), as shown in Figure 20B-D, it is concluded that β-ketoenamine COF still underperforms thiazole COF due to its inferior chemical stability. 163 Furthermore, it is noted that the out-of-plane flow of charge

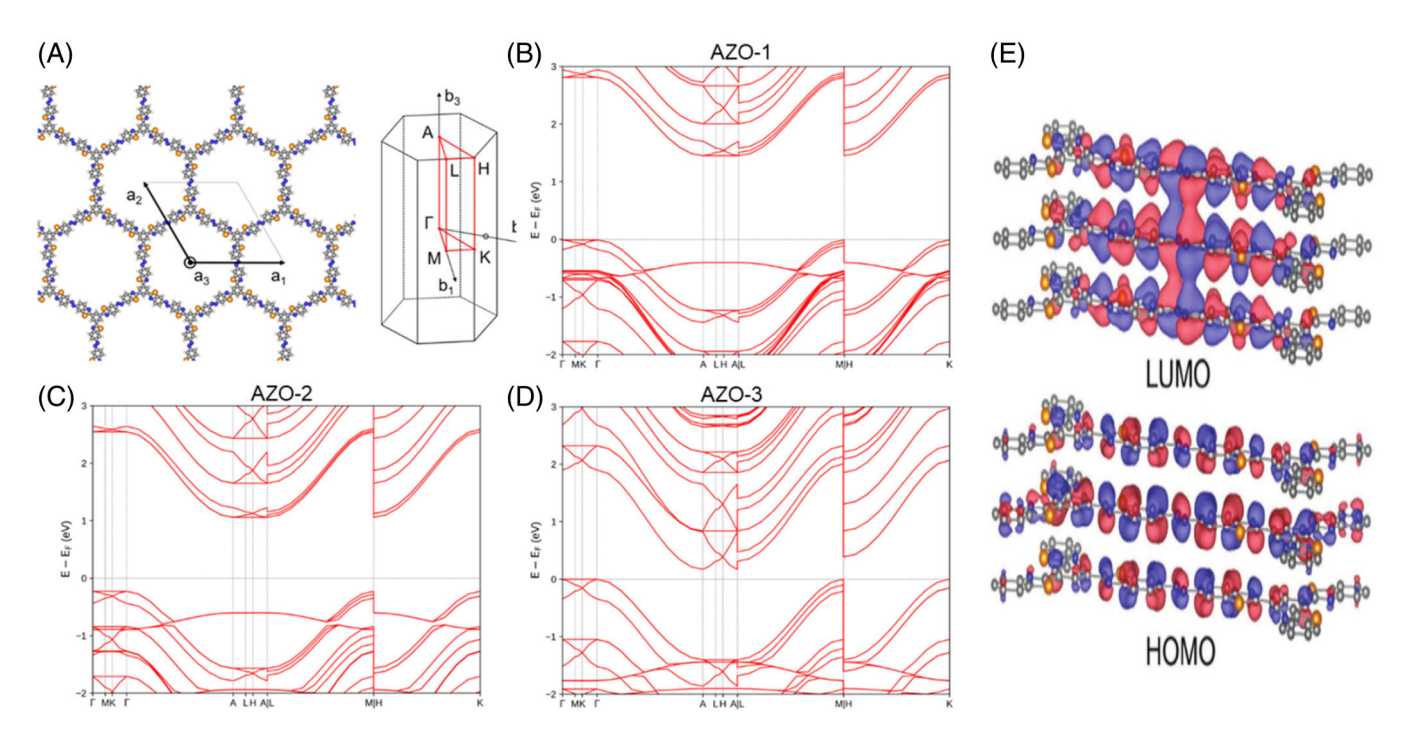


**FIGURE 20** Electronic structures of COFs with thiazole (AZO-1), imine (AZO-2), and β-ketoenamine (AZO-3) linkages are depicted. (A) Unit cell geometry of AZO-1 is shown, along with an illustration of high symmetry k-points of the COFs. (B–D) Using hybrid HSE06 functional, the band structure of AZO-1, AZO-2, and AZO-3 are computed. For AZO-1 and AZO-2, valence and conduction band edges are nearly flat along the in-plane direction to the COF plane (e.g.,  $\Gamma$ -M and K- $\Gamma$ ); furthermore, the direct band gap at the  $\Gamma$  point is farther than that of the indirect gap along  $\Gamma$ A path. This indicates that the in-plane direction flow of the charge carrier is not preferred over out-of-plane in the COFs. (E) Depiction of HOMO and LUMO orbitals of AZO-1. As shown, LUMO orbitals of azo groups between the layers have strong electronic coupling.  $^{163}$  Reproduced with permission: Copyright 2021, Wiley-VCH GmbH

carriers in the modeled COFs is favorable in comparison to the in-plane flow, as clearly presented by the narrow energy gap between HOMO and LUMO bands along the  $\Gamma$ -A path. This is further evidenced by the strong degree of overlap between the frontier orbitals of the layered thiazole COF as illustrated in Figure 20E. This finding corroborates the excellent electrochemical performance of the thiazole-linked COF during cycling.

#### 5.2 | Li-S batteries

In addition to their utilization as alkali ion battery electrodes, computational methods have shed light on the application of COFs as *chemical traps* to reduce the rapid capacity fading issue in Li-S batteries which is due to the shuttle effect of lithium polysulfides (Li<sub>2</sub>S<sub>x</sub>) and the accumulation of electrically inert products on electrodes. Yoo et al. <sup>130</sup> proposed a "microporous COF net on mesoporous CNT net" hybrid chemical trap (*NN interlayer*) for Li<sub>2</sub>S<sub>x</sub>, in which the effect of the COF pore size on the binding of Li<sub>2</sub>S<sub>x</sub> (x = 1, 4, 6, or 8) was characterized using computational methods. Grand canonical Monte Carlo (GCMC) simulations were performed to obtain initial binding configurations of Li<sub>2</sub>S<sub>x</sub> on CNT and COF with micropores of

0.7 nm (COF-1) and 2.7 nm (COF-5). Experimental and simulated XRD patterns support eclipsed and staggered arrangements for COF-5 and COF-1, respectively. 130 Based on these configurations, GCMC simulations reveal that COF-1 is capable of exclusively capturing Li<sub>2</sub>S, unlike COF-5 which was shown to accommodate the larger-sized  $\text{Li}_2S_x$  (x = 4, 6, and 8) as well as  $\text{Li}_2S$ . Furthermore, DFT calculations indicate that the Li<sub>2</sub>S has significantly higher bond energy with COF-1 compared to CNT and COF-5, with boron as the anchoring point. 130 Remarkably, COF-1 NN interlayer presented superior cyclic stability relative to COF-5 NN interlayer, which is attributed to the interaction of COF-5 with all Li<sub>2</sub>S<sub>x</sub> species resulting in the electrical isolation of incompletely oxidized polysulfide residuals and thereby leading to the degraded performance.<sup>130</sup> Unlike the previous report, <sup>130</sup> Song and colleagues<sup>164</sup> examined the nonstaggered AA stacking arrangement for COF-1. The optPBE-vDW functional 165 was employed to further investigate the interaction of polysulfides on the surface of COF-1 and COF-5.164 Using this approach, it is found that the polysulfide species, Li<sub>2</sub>S<sub>4</sub> and Li<sub>2</sub>S<sub>6</sub>, are further stabilized by the phenylene ring active site in addition to interaction with the O atom in the boroxine, confirming that COF-1 generally has a stronger interaction with the polysulfides which can

constrain the shuttle effect.<sup>164</sup> Therefore, the aforementioned studies illustrated how computational approaches can complement experimentation by providing more detailed information about the polysulfide anchoring mechanisms of different COFs.

# 5.3 | COF geometry—energy storage relationships

Understanding the structure-dependent electrochemistry of the COFs is essential for designing new COFs with enhanced energy storage capacity. For instance, since the strong  $\pi$ - $\pi$  interactions between the COF layers restrain the COF dissolution in electrolytes and improve conductivity, 163 the increase in COF stacking thickness affects cycling stability. Specifically, the control of COF stacking thickness seems to be an effective strategy to tune the reactivity and stability of the radical intermediates formed on the COF during discharge/charge processes. 46,118 It is noted that the initiation and transformation of C-O and  $\alpha$ -C radical intermediates take place during the redox processes as confirmed using electron paramagnetic resonance (EPR) and DFT calculations. 118 The capability of the  $\alpha$ -C radicals in COF to accommodate alkali metal ions was also confirmed recently through DFT computations of MESP. 166 Therefore, harnessing the reactivity and availability of these radical intermediates is crucial to the stability and performance of the COF electrodes. For instance, Gu et al. 118 demonstrated that increasing the stacking thickness of DAAQ-COF results in a higher degree of extinction and deactivation of the  $\alpha$ -C radical intermediates due to increased self-discharge of the radicals during the redox process. This interesting finding evidently indicates that the reactivity and stability of radical intermediates can be tuned by modulating the thickness of COF nanosheets. 118

Due to the strong  $\pi$ - $\pi$  interactions between eclipsed COF stacks, the storage capacity could be suboptimal due to the inhibition of Li-ion infiltration and diffusion into the interior active sites that are buried deeply inside the COF stacks, implying that the delamination of COFs would improve ion migration. 48,65 Lei and coworkers have investigated a COF-CNT hybrid system as an alternative to mechanical exfoliation for LIBs for more effective utilization of redox-active sites. 48 MD simulations confirmed that COF wraps around CNT through the  $\pi$ - $\pi$ interactions. In their study, DFT was also used to investigate the lithium storage mechanism in the COF monomers.48 It is found that Li-ions are preferentially bound to the nitrogen atoms of imine (C=N) functional groups, and then at the carbon atoms of phenylene rings, which yields a 14 Li-ion accommodation for each monomer of COF. Although MD simulations indicate that the distance between COF and CNT is increased slightly during Li-ion insertion, it is found that even fully lithiated COF remains within ~3.7 Å from CNT, meaning that the  $\pi$ - $\pi$  interaction is still intact. Therefore, it was suggested that such expansion of interlamellar spacing during cycling leads to the improved lithiation/delithiation kinetics at the phenylene rings as well as the attainment of the maximum Li-ion accommodation (up to 14 Li-ions).  $^{48}$ 

More recently, Nagai and coworkers investigated four different polyimide COFs consisting of aromatic dianhydrides active parts (pyromellitic dianhydride (PMDA) or 1,4,5,8-naphthalenetetracarboxylic dianhydride (NTCDA)) and aromatic triamines linkers (tris(4-aminophenyl)amine (TAPA) or 1.3.5-tris(4-aminophenyl)benzene (TAPB)). 158 By considering the energy change as a function of torsion angle between the phenylene group of TAPA and TAPB, DFT calculations exhibit that it is energetically favorable for the phenylene rings in both linkage molecules to be tilted to have equal torsion angles with one another as shown in Figure 21A. 158 This is in contrast with the flat 2D configuration that has often been portrayed in literature. This torsion of the triamine linkers is significant in affecting the interlayer spacing between the COFs as well as the pore size, shape, and elongation of the pore walls which are the factors affecting ion mobility and infiltration into the inner active sites through the COF layers.

The preferred stacking configuration of COFs is another significant feature affecting electrochemical performance and stability, which has been studied using computational methods. Previously, it was reported that the COFs consisting of TAPB-PMDA or TAPA-PMDA likely prefer serrated stacking rather than eclipsed or staggered configurations. 152 However, it should be noted that the simulated PXRD patterns for both the eclipsed and serrated configurations seem to agree with experimental patterns. 152 Therefore, further calculations were required to determine the preferred stacking configuration. Nagai et al. examined the stacking preference of the COFs as shown in Figures 21B-D, demonstrating that the eclipsed configuration is the most energetically favorable. 158 However, for the COF consisting of TAPA-NTCDA, the energy did not increase monotonously as the COF was shifted from fully eclipsed to fully staggered stacking; instead a local energy minimum was discovered between eclipsed and staggered stackings as a metastable serrated-stacking orientation (Figure 21E). 158 This might suggest that during the charge or discharge of a battery, the COF orientations may shift between these configurations and thereby affect the mobility of ions. Possibly, the stacking of the COF may be modified during the binding of alkali metal ions with active sites due to the low energy barrier for changing the configurations.<sup>158</sup> In fact, it is found that for

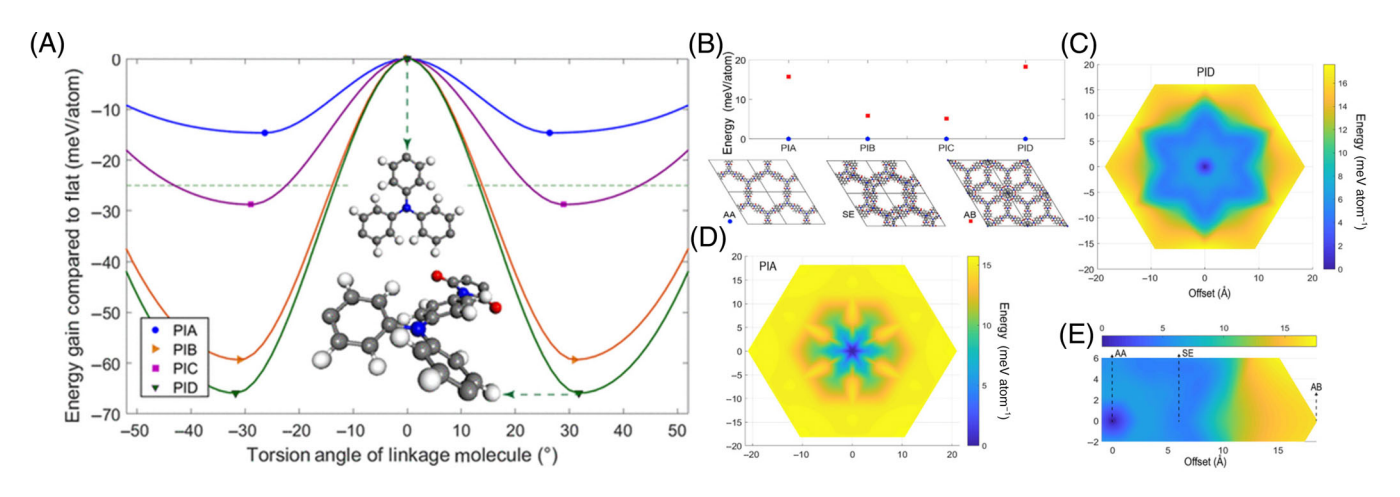
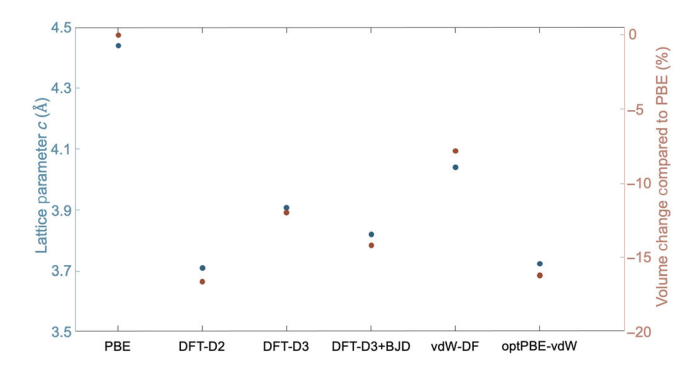


FIGURE 21 (A) Energy landscape (relative to flat configuration) as a function of torsion angle between the benzene rings of the linkage molecule of four COFs (PIA  $\rightarrow$  TAPB/PMDA; PIB  $\rightarrow$  TAPA/PMDA; PIC  $\rightarrow$  TAPB/NTCDA; PID  $\rightarrow$  TAPA/NTCDA). (B) The energy of AB staggered relative to eclipsed (AA) is shown, as well as illustrations of three stacking configurations of COF. Energy landscape obtained from a variety of offsets of the adjacent sheets of (C) PID and (D) PIA, where the corners of the hexagons represent the staggered (AB) configuration. (E) The energy landscape of PID offset along the direction toward the AB stacking is illustrated; a metastable serrated stacking (SE) is detected at an offset of 6.6 Å. 158 Reproduced with permission: Copyright 2021, American Chemical Society (further permissions related to the material excerpted should be directed to the ACS)



**FIGURE 22** The *c* lattice parameter and volume of PIB as computed by different DFT methods.<sup>158</sup> Adapted with permission: Copyright 2021, American Chemical Society (further permissions related to the material excerpted should be directed to the ACS)

TAPB-NTCDA based COF the reduction and oxidation peaks increase slightly versus Na/Na<sup>+</sup> after the first scan; this could be due to a shift of the COF stacking to a more energetically favorable and electrochemically active configuration, resulting in the increase of the redox potential.<sup>158</sup>

Due to their high degree of structural tunability, the electronic properties of COF can be more deliberately modulated to suit various applications including optoelectronics and energy storage. Namely, the band gap of the COF can be engineered to enhance the conductivity of the COF thereby improving the Coulombic efficiency of the battery, or to achieve tunable light emission for optoelectronics. Using the DFT method, Zhu and Meunier have shown that the band gaps of COFs are sensitive to the length of the organic bridging ligand, as well as to the applied

mechanical strain.<sup>167</sup> It was shown that the band gap of COF-1 can be decreased by increasing the number of phenylene rings separating the boroxine nodes. This is because the modulation of the phenylene chain size affects the features of the valence band maximum (VBM), while having a minimal effect on the conduction band minimum (CBM) whose electronic density is primarily localized around the nodes.<sup>167</sup> On the other hand, as an alternative to modifying the structure of the COF, it has been shown that the band gap can be modulated by the intercalation of iron<sup>168,169</sup> and first-row transition metals.<sup>170</sup>

The structural change of the COFs with alkali atom loading is another important topic for computational studies. For instance, to investigate the interaction of intercalated Li atoms in COF and their effect on electronic properties, Fang and coworkers142 conducted a computational study on NUS-2 COF anode, 171 presenting that the volume of *n*Li-NUS2 is gradually decreased with increasing Li loading (n up to 12). This trend could be due to an enhanced interlayer interaction of COF in the presence of Li. 142 Additionally, it was shown that the Li atoms preferentially bind to the carbonyl oxygens. Once the carbonyl sites are occupied, additional Li atoms are distributed within the micropore. 142 Notably, the Li-Li distances reported for the Li atoms are slightly longer in the micropore than that of Li dimer, possibly suggesting that NUS-2 COF suppresses the formation of Li<sub>2</sub>. 142

Despite the usefulness of computational approaches for providing insight at the atomistic scale, it has been well known that calculated results can be quite sensitive to the level of theory employed in computational studies, which has a significant impact on the accuracy of the predictions. For instance, as shown in Figure 22, due to the inadequate incorporation of vDW interactions, DFT calculations using PBE<sup>172</sup> may result in a significant overestimation of the COF interlayer spacing.<sup>158</sup> In contrast, PBE with DFT-D3 method of Grimme<sup>173</sup> or optPBE-vdW<sup>165</sup> can provide significant accuracy improvement in assessing the interlayer spacing and configuration of COFs. Since the interlayer spacing is critical to account for ion infiltration into the pores as well as the out-of-plane conductivity in COF, first-principles approaches investigating COF should take into account the long-range dispersion interactions for more accurate geometry and electronic predictions.

#### 6 | CONCLUSION AND OUTLOOK

Over the past few years, tremendous progress has been achieved in the development of COFs as high-performance functional materials for energy storage devices, making them promising options for environmentally friendly energy systems. In this review, we have summarized recent advances on COF regarding its working principle, synthesis method, effective design strategies, and computational studies in energy storage applications including supercapacitor and various battery systems. While the unique properties of COFs offer great potential and opportunity, the research in this field is still at the beginning stage with many imminent challenges.

As the active material for supercapacitors and batteries, efficient molecular design of COFs is necessary to maximize their redox activity. Aside from a few exceptions, <sup>48,49,51</sup> most redox-active COFs reported so far have chosen to use a combination of redox-active and inactive building blocks to satisfy the reaction pathway for the COF assembly. Consequently, the theoretical capacity of the COFs is significantly reduced and generally less than those of the redox-active molecule in monomer form, imposing severe limits on the gravimetric energy density of COF-based electrodes. Therefore, designing COFs that contain a higher density of redox-active sites while maintaining sufficient physical and chemical stability in the working environment is critical for achieving the high electrochemical performance of the COF electrodes.

Besides increasing the number of active sites in the framework, improving the accessibility of the redoxactive sites in the bulk region of COF electrodes also has a significant impact on the practical charge storage performance in EES devices. Although COFs possess a uniform porous structure, it was found that the nanochannels formed by the aligned COF stacks also exhibit poor ion transport properties, leading to poor

utilization of redox-active sites. In that regard, exfoliation of COF into nanosheets is effective in improving the utilization level of redox-active sites by shortening the ion transport pathway and increasing the number of exposed redox-active sites on the exposed surface. However, although several exfoliation methods have been reported and applied to CON synthesis for EES devices, exfoliation of COFs to CONs with high crystallinity and atomic level of control remains a daunting task. To achieve precise manipulation of key physical parameters including crystallinity, size, stacking pattern, and orientation, the dynamics of COF structural evolution over the exfoliation process still require further investigation.

Electronic and ionic conductivity are also important parameters for the rate performance of EES devices. Charge conduction of COFs can be influenced by numerous factors including choice of charge carrier, charge state of COF, porosity, orientation, and degree of crystallinity. In particular, the low electronic conductivity has been a critical flaw to overcome for COF-based electrodes. In that respect, COFs designed with an extended  $\pi$ -conjugated skeleton and strong interlayer orbital stacking are desirable and expected to exhibit superior electronic properties and rate performance in EES systems. The utilization of conductive substrate for electrode preparation is another direct method to improve electronic conductivity at the expense of reducing specific capacity. As solid electrolytes, the ion conduction of COFs has been primarily studied with Liions, and structural modification strategies such as crystal alignment and ionic framework have been investigated. However, the conduction behavior of COFs with other ions applicable to EES systems has not yet been investigated, and the correlation between the physical parameters of COFs and transport properties is still unclear.

There are also many practical challenges that COFs are facing in design and synthesis. While numerous accelerated synthesis methods have been reported, their compatibility with the broad range of reaction pathways and the quality of the crystal are often unclear. The uniform porosity of COFs is a unique structural feature that can bring both burden and opportunity. Because of the nature of their porous framework, redox-active COFs typically have low energy and power density per volume due to their low packing density. The accessibility of the active site in the bulk region is also restricted owing to limited ion mobility in the pores. However, the pores and nanochannels formed within the void space offer tremendous design space that may be utilized to enhance the electrochemical properties by incorporating other substances or modifications to the framework in postprocesses. For example, conductive polymers embedded or grafted in the nanochannels have been demonstrated to enhance charge storage and conductive properties. Since

the nanopores are confined within the framework, modifications to this space are more efficient and favorable compared to those outside the COF structure. Additionally, more complex COF topologies such as 3D structure and 2D heterostructures could lead to more desirable electrochemical properties with 3D interconnected charge transport channels or hierarchically porous frameworks.

The fundamental charge storage mechanisms of the redox-active COFs and their kinetic properties also need further investigation. Such topics could yield substantial insights from the collaboration between experimental and computational studies. We have reviewed a collection of recent computational studies aimed at providing a fundamental understanding of the electrochemical behaviors of COFs. Coupled with increasingly available depositories of data, as well as algorithmic breakthroughs in computational materials science and rapidly enhanced computational power, machine learning has been thriving in recent years. 174-178 In conjunction with high-throughput computational approaches, such studies can immensely expedite the exploration of novel COF development for energy storage applications. 178,179 Although there have yet to be sufficient machine learning studies aimed at further elucidating the structure-electrochemical property relationship of COFs, it is anticipated that the machine learning approach will guide research to efficiently achieve the desirable properties and performances of COFs through finely tuned designs of their chemical structures.

In conclusion, studies in COFs offer a promising material platform for designing advanced organic EES devices. To deepen the understanding of the structureproperty relationships of COFs and overcome the challenges of applying them to EES devices, we propose the following topics for future research: (1) increase number of redox-active sites in the framework; (2) improve charge transport properties with precise structural adjustment and postmodifications; (3) exploit the utility of vacancies in lattice for enhanced performance and multifunctionalities; (4) design and evaluate 2D heterostructural and 3D COFs for EES application; (5) develop more efficient and scalable synthesis methods for highly crystalline COFs; (6) systematically investigate the fundamental structure-properties relationships with experimental and computational studies; (7) accelerate the design and preparation of high-performance COFs with computationally-driven optimization.

#### **CONFLICT OF INTEREST**

The authors declare no conflict of interest.

#### ORCID

Seung Woo Lee https://orcid.org/0000-0002-2695-7105

#### REFERENCES

- Larcher D, Tarascon JM. Towards greener and more sustainable batteries for electrical energy storage. Nat Chem. 2015; 7(1):19-29.
- Liang YL, Yao Y. Positioning organic electrode materials in the battery landscape. *Joule*. 2018;2(9):1690-1706.
- Schon TB, McAllister BT, Li PF, Seferos DS. The rise of organic electrode materials for energy storage. *Chem Soc Rev.* 2016;45(22):6345-6404.
- Wang H, Yao CJ, Nie HJ, et al. Recent progress in carbonylbased organic polymers as promising electrode materials for lithium-ion batteries (LIBs). J Mater Chem A. 2020;8(24): 11906-11922.
- Lee S, Kwon G, Ku K, et al. Recent progress in organic electrodes for Li and Na rechargeable batteries. Adv Mater. 2018; 30(42):1704682.
- Lu Y, Zhang Q, Li L, Niu ZQ, Chen J. Design strategies toward enhancing the performance of organic electrode materials in metal-ion batteries. *Chem.* 2018;4(12):2786-2813.
- 7. Cote AP, Benin AI, Ockwig NW, O'Keeffe M, Matzger AJ, Yaghi OM. Porous, crystalline, covalent organic frameworks. *Science*. 2005;310(5751):1166-1170.
- Diercks CS, Yaghi OM. The atom, the molecule, and the covalent organic framework. *Science*. 2017;355(6328):eaal1585.
- 9. Furukawa H, Yaghi OM. Storage of hydrogen, methane, and carbon dioxide in highly porous covalent organic frameworks for clean energy applications. *J Am Chem Soc.* 2009;131(25): 8875-8883.
- 10. Han SS, Furukawa H, Yaghi OM, Goddard WA. Covalent organic frameworks as exceptional hydrogen storage materials. *J Am Chem Soc.* 2008;130(35):11580-11581.
- 11. Zeng YF, Zou RQ, Zhao YL. Covalent organic frameworks for CO2 capture. *Adv Mater.* 2016;28(15):2855-2873.
- 12. Fan HW, Mundstock A, Feldhoff A, et al. Covalent organic framework-covalent organic framework bilayer membranes for highly selective gas separation. *J Am Chem Soc.* 2018; 140(32):10094-10098.
- Wang ZF, Zhang SN, Chen Y, Zhang ZJ, Ma SQ. Covalent organic frameworks for separation applications. *Chem Soc Rev.* 2020;49(3):708-735.
- 14. Rogge SMJ, Bavykina A, Hajek J, et al. Metal-organic and covalent organic frameworks as single-site catalysts. *Chem Soc Rev.* 2017;46(11):3134-3184.
- 15. Zhi YF, Wang ZR, Zhang HL, Zhang QC. Recent progress in metal-free covalent organic frameworks as heterogeneous catalysts. *Small.* 2020;16(24):202001070.
- 16. Lin S, Diercks CS, Zhang YB, et al. Covalent organic frameworks comprising cobalt porphyrins for catalytic CO2 reduction in water. *Science*. 2015;349(6253):1208-1213.
- 17. Liu XG, Huang DL, Lai C, et al. Recent advances in covalent organic frameworks (COFs) as a smart sensing material. *Chem Soc Rev.* 2019;48(20):5266-5302.
- Wang JL, Zhuang ST. Covalent organic frameworks (COFs) for environmental applications. Coord Chem Rev. 2019;400: 213046
- Peng YW, Huang Y, Zhu YH, et al. Ultrathin two-dimensional covalent organic framework nanosheets: preparation and application in highly sensitive and selective DNA detection. *J Am Chem Soc.* 2017;139(25):8698-8704.

- Zhang CL, Zhang SM, Yan YH, Xia F, Huang AN, Xian YZ. Highly fluorescent polyimide covalent organic nanosheets as sensing probes for the detection of 2,4,6-trinitrophenol. ACS Appl Mater Interfaces. 2017;9(15):13415-13421.
- Keller N, Bein T. Optoelectronic processes in covalent organic frameworks. Chem Soc Rev. 2021;50(3):1813-1845.
- Dai CH, Liu B. Conjugated polymers for visible-light-driven photocatalysis. *Energ Environ Sci.* 2020;13(1):24-52.
- Xu S, Zhang Q. Recent progress in covalent organic frameworks as light-emitting materials. *Mater Today Energy*. 2021; 20:100635.
- Yu F, Liu WB, Ke SW, Kurmoo M, Zuo JL, Zhang QC. Electrochromic two-dimensional covalent organic framework with a reversible dark-to-transparent switch. *Nat Commun.* 2020; 11(1):5534.
- Yu F, Liu WB, Li B, Tian D, Zuo JL, Zhang QC. Photostimulus-responsive large-area two-dimensional covalent organic framework films. *Angew Chem Int Ed.* 2019;58(45): 16101-16104.
- She PF, Qin YY, Wang X, Zhang QC. Recent Progress in external-stimulus-responsive 2D covalent organic frameworks. Adv Mater. 2021;2101175.
- Fang QR, Wang JH, Gu S, et al. 3D porous crystalline polyimide covalent organic frameworks for drug delivery. *J Am Chem Soc.* 2015;137(26):8352-8355.
- Mitra S, Sasmal HS, Kundu T, et al. Targeted drug delivery in covalent organic Nanosheets (CONs) via sequential postsynthetic modification. *J Am Chem Soc.* 2017;139(12):4513-4520.
- Scicluna MC, Vella-Zarb L. Evolution of nanocarrier drug-delivery systems and recent advancements in covalent organic frameworkdrug systems. ACS Appl Nano Mater. 2020;3(4):3097-3115.
- Zhan XJ, Chen Z, Zhang QC. Recent progress in twodimensional COFs for energy-related applications. *J Mater Chem A*. 2017;5(28):14463-14479.
- 31. Li J, Jing XC, Li QQ, et al. Bulk COFs and COF nanosheets for electrochemical energy storage and conversion. *Chem Soc Rev.* 2020;49(11):3565-3604.
- 32. Wang DG, Qiu TJ, Guo WH, et al. Covalent organic framework-based materials for energy applications. *Energ Environ Sci.* 2021;14(2):688-728.
- Wu JL, Xu F, Li SM, et al. Porous polymers as multifunctional material platforms toward task-specific applications. Adv Mater. 2019;31(4):1802922.
- 34. Song YP, Sun Q, Aguila B, Ma SQ. Opportunities of covalent organic frameworks for advanced applications. *Adv Sci.* 2019; 6(2):1801410.
- 35. Li BQ, Zhang SY, Wang B, Xia ZJ, Tang C, Zhang Q. A porphyrin covalent organic framework cathode for flexible Zn-air batteries. *Energ Environ Sci.* 2018;11(7):1723-1729.
- Park JH, Lee CH, Ju JM, et al. Bifunctional covalent organic framework-derived electrocatalysts with modulated p-band centers for rechargeable Zn-air batteries. Adv Funct Mater. 2021;31(25):2101727.
- 37. Peng P, Shi L, Huo F, et al. In situ charge exfoliated soluble covalent organic framework directly used for Zn-air flow battery. *ACS Nano*. 2019;13(1):878-884.
- 38. Liu C, Liu F, Li H, et al. One-dimensional van der Waals heterostructures as efficient metal-free oxygen electrocatalysts. *ACS Nano*. 2021;15(2):3309-3319.

- Cui X, Lei S, Wang AC, et al. Emerging covalent organic frameworks tailored materials for electrocatalysis. *Nano Energy*. 2020;70:104525.
- Zhao XJ, Pachfule P, Thomas A. Covalent organic frameworks (COFs) for electrochemical applications. *Chem Soc Rev.* 2021; 50(12):6871-6913.
- 41. Li M, Liu JJ, Zhang T, Song XY, Chen WH, Chen L. 2D redoxactive covalent organic frameworks for supercapacitors: design, synthesis, and challenges. *Small*. 2021;17(22):2005073.
- 42. Wang H, Zeng ZT, Xu P, et al. Recent progress in covalent organic framework thin films: fabrications, applications and perspectives. *Chem Soc Rev.* 2019;48(2):488-516.
- Lohse MS, Bein T. Covalent organic frameworks: structures, synthesis, and applications. Adv Funct Mater. 2018;28(33): 1705553.
- Kandambeth S, Dey K, Banerjee R. Covalent organic frameworks: chemistry beyond the structure. *J Am Chem Soc.* 2019; 141(5):1807-1822.
- 45. Huang N, Wang P, Jiang DL. Covalent organic frameworks: a materials platform for structural and functional designs. *Nat Rev Mater.* 2016;1(10):16068.
- Sun T, Xie J, Guo W, Li DS, Zhang QC. Covalent-organic frameworks: advanced organic electrode materials for rechargeable batteries. Adv Energy Mater. 2020;10(19):1904199.
- Jin YH, Yu C, Denman RJ, Zhang W. Recent advances in dynamic covalent chemistry. *Chem Soc Rev.* 2013;42(16):6634-6654.
- Lei ZD, Yang QS, Xu Y, et al. Boosting lithium storage in covalent organic framework via activation of 14-electron redox chemistry. *Nat Commun.* 2018;9(1):576.
- Shi RJ, Liu LJ, Lu Y, et al. Nitrogen-rich covalent organic frameworks with multiple carbonyls for high-performance sodium batteries. *Nat Commun*. 2020;11(1):178.
- Luo ZQ, Liu LJ, Ning JX, et al. A microporous covalentorganic framework with abundant accessible carbonyl groups for lithium-ion batteries. *Angew Chem Int Ed.* 2018;57(30): 9443-9446.
- Zhao GF, Zhang YY, Gao ZH, et al. Dual active site of the azo and carbonyl-modified covalent organic framework for highperformance Li storage. ACS Energy Lett. 2020;5(4):1022-1031.
- Zeng YF, Zou RY, Luo Z, et al. Covalent organic frameworks formed with two types of covalent bonds based on orthogonal reactions. *J Am Chem Soc.* 2015;137(3):1020-1023.
- Pang ZF, Xu SQ, Zhou TY, Liang RR, Zhan TG, Zhao X. Construction of covalent organic frameworks bearing three different kinds of pores through the heterostructural mixed linker strategy. J Am Chem Soc. 2016;138(14):4710-4713.
- 54. Xiao ZB, Li LY, Tang YJ, et al. Covalent organic frameworks with lithiophilic and sulfiphilic dual linkages for cooperative affinity to polysulfides in lithium-sulfur batteries. *Energy Storage Mater*. 2018;12:252-259.
- Kandambeth S, Venkatesh V, Shinde DB, et al. Self-templated chemically stable hollow spherical covalent organic framework. *Nat Commun*. 2015;6(1):6786.
- Jin EQ, Asada M, Xu Q, et al. Two-dimensional sp(2) carbonconjugated covalent organic frameworks. *Science*. 2017; 357(6352):673-676.
- 57. Liu W, Luo X, Bao Y, et al. A two-dimensional conjugated aromatic polymer via C-C coupling reaction. *Nat Chem.* 2017; 9(6):563-570.

- Xu YH, Jin SB, Xu H, Nagai A, Jiang DL. Conjugated microporous polymers: design, synthesis and application. *Chem Soc Rev.* 2013;42(20):8012-8031.
- 59. Jiang JX, Su F, Trewin A, et al. Conjugated microporous poly (aryleneethynylene) networks. *Angew Chem Int Ed.* 2007; 46(45):8574-8578.
- Biswal BP, Chandra S, Kandambeth S, Lukose B, Heine T, Banerjeet R. Mechanochemical synthesis of chemically stable isoreticular covalent organic frameworks. *J Am Chem Soc.* 2013;135(14):5328-5331.
- Jin EQ, Li J, Geng KY, et al. Designed synthesis of stable light-emitting two-dimensional sp(2) carbon-conjugated covalent organic frameworks. *Nat Commun.* 2018;9(1):4143.
- Muench S, Wild A, Friebe C, Haupler B, Janoschka T, Schubert US. Polymer-based organic batteries. *Chem Rev.* 2016;116(16):9438-9484.
- 63. DeBlase CR, Silberstein KE, Truong TT, Abruna HD, Dichtel WR. Beta-ketoenamine-linked covalent organic frameworks capable of pseudocapacitive energy storage. *J Am Chem Soc.* 2013;135(45):16821-16824.
- 64. Yang CX, Liu C, Cao YM, Yan XP. Facile room-temperature solution-phase synthesis of a spherical covalent organic framework for high-resolution chromatographic separation. *Chem Commun.* 2015;51(61):12254-12257.
- 65. Wang S, Wang QY, Shao PP, et al. Exfoliation of covalent organic frameworks into few-layer redox-active nanosheets as cathode materials for lithium-ion batteries. *J Am Chem Soc.* 2017;139(12):4258-4261.
- Colson JW, Woll AR, Mukherjee A, et al. Oriented 2D covalent organic framework thin films on single-layer graphene. *Science*. 2011;332(6026):228-231.
- 67. Peng YW, Wong WK, Hu ZG, et al. Room temperature batch and continuous flow synthesis of water-stable covalent organic frameworks (COFs). *Chem Mater.* 2016;28(14):5095-5101.
- 68. Guan XY, Ma YC, Li H, et al. Fast, ambient temperature and pressure lonothermal synthesis of three-dimensional covalent organic frameworks. *J Am Chem Soc.* 2018;140(13):4494-4498.
- 69. Matsumoto M, Valentino L, Stiehl GM, et al. Lewis-acid-catalyzed interfacial polymerization of covalent organic framework films. *Chem.* 2018;4(2):308-317.
- Hao Q, Zhao CQ, Sun B, et al. Confined synthesis of twodimensional covalent organic framework thin films within superspreading water layer. J Am Chem Soc. 2018;140(38): 12152-12158.
- 71. Wang R, Shi XS, Xiao AK, Zhou W, Wang Y. Interfacial polymerization of covalent organic frameworks (COFs) on polymeric substrates for molecular separations. *J Membr Sci.* 2018; 566:197-204.
- Yang L, Guo QY, Kang H, Chen RZ, Liu YQ, Wei DC. Selfcontrolled growth of covalent organic frameworks by repolymerization. *Chem Mater.* 2020;32(13):5634-5640.
- 73. Dai WY, Shao F, Szczerbinski J, et al. Synthesis of a twodimensional covalent organic monolayer through dynamic imine chemistry at the air/water Interface. *Angew Chem Int Ed.* 2016;55(1):213-217.
- 74. Campbell NL, Clowes R, Ritchie LK, Cooper AI. Rapid microwave synthesis and purification of porous covalent organic frameworks. *Chem Mater.* 2009;21(2):204-206.

- 75. Wei H, Chai SZ, Hu NT, Yang Z, Wei LM, Wang L. The microwave-assisted solvothermal synthesis of a crystalline two-dimensional covalent organic framework with high CO2 capacity. *Chem Commun*. 2015;51(61):12178-12181.
- Ritchie LK, Trewin A, Reguera-Galan A, Hasell T, Cooper AI. Synthesis of COF-5 using microwave irradiation and conventional solvothermal routes. *Microporous Mesoporous Mater*. 2010;132(1–2):132-136.
- 77. Yang ST, Kim J, Cho HY, Kim S, Ahn WS. Facile synthesis of covalent organic frameworks COF-1 and COF-5 by sonochemical method. *RSC Adv.* 2012;2(27):10179-10181.
- Medina DD, Rotter JM, Hu YH, et al. Room temperature synthesis of covalent-organic framework films through vapor-assisted conversion. J Am Chem Soc. 2015;137(3):1016-1019.
- DeBlase CR, Hernandez-Burgos K, Silberstein KE, et al. Rapid and efficient redox processes within 2D covalent organic framework thin films. ACS Nano. 2015;9(3):3178-3183.
- 80. DeBlase CR, Hernandez-Burgos K, Rotter JM, et al. Cation-dependent stabilization of electrogenerated naphthalene diimide dianions in porous polymer thin films and their application to electrical energy storage. *Angew Chem.* 2015;54(45): 13225-13229.
- Hao L, Ning J, Luo B, et al. Structural evolution of 2D microporous covalent triazine-based framework toward the study of high-performance supercapacitors. *J Am Chem Soc.* 2015; 137(1):219-225.
- 82. El-Mahdy AFM, Mohamed MG, Mansoure TH, Yu HH, Chen T, Kuo SW. Ultrastable tetraphenyl-pphenylenediaminebased covalent organic frameworks as platforms for high-performance electrochemical supercapacitors. *Chem Commun.* 2019;55(99):14890-14893.
- 83. Khattak AM, Ghazi ZA, Liang B, et al. A redox-active 2D covalent organic framework with pyridine moieties capable of faradaic energy storage. *J Mater Chem A*. 2016;4(42):16312-16317.
- 84. Khayum MA, Vijayakumar V, Karak S, et al. Convergent covalent organic framework thin sheets as flexible supercapacitor electrodes. *ACS Appl Mater Interfaces*. 2018;10(33): 28139-28146.
- 85. Chandra S, Chowdhury DR, Addicoat M, Heine T, Paul A, Banerjee R. Molecular level control of the capacitance of two-dimensional covalent organic frameworks: role of hydrogen bonding in energy storage materials. *Chem Mater.* 2017;29(5): 2074-2080.
- 86. Halder A, Ghosh M, Khayum MA, et al. Interlayer hydrogenbonded covalent organic frameworks as high-performance supercapacitors. *J Am Chem Soc.* 2018;140(35):10941-10945.
- 87. Li L, Lu F, Xue R, et al. Ultrastable triazine-based covalent organic framework with an interlayer hydrogen bonding for supercapacitor applications. *ACS Appl Mater Interfaces*. 2019; 11(29):26355-26363.
- 88. Yusran Y, Li H, Guan XY, et al. Exfoliated mesoporous 2D covalent organic frameworks for high-rate electrochemical double-layer capacitors. *Adv Mater.* 2020;32(8):1907289.
- 89. Xu F, Xu H, Chen X, et al. Radical covalent organic frameworks: a general strategy to immobilize open-accessible polyradicals for high-performance capacitive energy storage. *Angew Chem Int Ed.* 2015;54(23):6814-6818.

- 90. Mulzer CR, Shen LX, Bisbey RP, et al. Superior charge storage and power density of a conducting polymer-modified covalent organic framework. *ACS Cent Sci.* 2016;2(9):667-673.
- 91. Wu Y, Yan DW, Zhang ZY, Matsushita MM, Awaga K. Electron highways into nanochannels of covalent organic frameworks for high electrical conductivity and energy storage. *ACS Appl Mater Interfaces*. 2019;11(8):7661-7665.
- Liu S, Yao L, Lu Y, et al. All-organic covalent organic framework/polyaniline composites as stable electrode for high-performance supercapacitors. *Mater Lett.* 2019;236: 354-357.
- 93. Han Y, Hu NT, Liu S, et al. Nanocoating covalent organic frameworks on nickel nanowires for greatly enhancedperformance supercapacitors. *Nanotechnology*. 2017;28(33):33LT01.
- Sun B, Liu J, Cao AM, Song WG, Wang D. Interfacial synthesis of ordered and stable covalent organic frameworks on amino-functionalized carbon nanotubes with enhanced electrochemical performance. *Chem Commun.* 2017;53(47):6303-6306
- 95. Xu JS, He YF, Bi S, et al. An olefin-linked covalent organic framework as a flexible thin-film electrode for a high-performance micro-supercapacitor. *Angew Chem Int Ed.* 2019; 58(35):12065-12069.
- Zha ZQ, Xu LR, Wang ZK, et al. 3D Graphene functionalized by covalent organic framework thin film as capacitive electrode in alkaline media. ACS Appl Mater Interfaces. 2015; 7(32):17837-17843.
- 97. Xu LR, Wang F, Ge X, Liu RY, Xu M, Yang JQ. Covalent organic frameworks on reduced graphene oxide with enhanced electrochemical performance. *Microporous Mesoporous Mater.* 2019;287:65-70.
- Wang PY, Wu Q, Han LF, et al. Synthesis of conjugated covalent organic frameworks/graphene composite for supercapacitor electrodes. RSC Adv. 2015;5(35):27290-27294.
- 99. Li CX, Yang J, Pachfule P, et al. Ultralight covalent organic framework/graphene aerogels with hierarchical porosity. *Nat Commun*. 2020;11(1):4712.
- 100. An N, Guo Z, Xin J, et al. Hierarchical porous covalent organic framework/graphene aerogel electrode for highperformance supercapacitors. J Mater Chem A. 2021;9(31): 16824-16833.
- 101. Wang CJ, Liu F, Chen JS, et al. A graphene-covalent organic framework hybrid for high-performance supercapacitors. *Energy Storage Mater.* 2020;32:448-457.
- Haldar S, Kushwaha R, Maity R, Vaidhyanathan R. Pyridinerich covalent organic frameworks as high-performance solid-state Supercapacitors. ACS Mater Lett. 2019;1(4):490-497.
- 103. Guo XH, Tian Y, Zhang MC, et al. Mechanistic insight into hydrogen-bond-controlled crystallinity and adsorption property of covalent organic frameworks from flexible building blocks. Chem Mater. 2018;30(7):2299-2308.
- 104. Kandambeth S, Shinde DB, Panda MK, Lukose B, Heine T, Banerjee R. Enhancement of chemical stability and crystallinity in porphyrin-containing covalent organic frameworks by intramolecular hydrogen bonds. *Angew Chem Int Ed.* 2013; 52(49):13052-13056.
- 105. Xu F, Jin SB, Zhong H, et al. Electrochemically active, crystalline, mesoporous covalent organic frameworks on carbon

- nanotubes for synergistic lithium-ion battery energy storage. *Sci Rep.* 2015;5(1):8225.
- 106. Yang DH, Yao ZQ, Wu DH, Zhang YH, Zhou Z, Bu XH. Structure-modulated crystalline covalent organic frameworks as high-rate cathodes for Li-ion batteries. *J Mater Chem A*. 2016; 4(47):18621-18627.
- 107. Meng ZY, Zhang Y, Dong MQ, et al. Readily useable bulk phenoxazine-based covalent organic framework cathode materials with superior kinetics and high redox potentials. *J Mater Chem A*. 2021;9(17):10661-10665.
- 108. Schon TB, Tilley AJ, Kynaston EL, Seferos DS. Threedimensional arylene diimide frameworks for highly stable lithium ion batteries. ACS Appl Mater Interfaces. 2017;9(18): 15631-15637.
- 109. Wang ZL, Li YJ, Liu PJ, et al. Few layer covalent organic frameworks with graphene sheets as cathode materials for lithium-ion batteries. *Nanoscale*. 2019;11(12):5330-5335.
- Wang G, Chandrasekhar N, Biswal BP, et al. A crystalline, 2D polyarylimide cathode for ultrastable and ultrafast Li storage. *Adv Mater*. 2019;31(28):1901478.
- Yao CJ, Wu ZZ, Xie J, et al. Two-dimensional (2D) covalent organic framework as efficient cathode for binder-free lithium-ion battery. *ChemSusChem.* 2020;13(9):2457-2463.
- 112. Yang H, Zhang SL, Han LH, et al. High conductive twodimensional covalent organic framework for lithium storage with large capacity. *ACS Appl Mater Interfaces*. 2016;8(8):5366-5375.
- Bai LY, Gao Q, Zhao YL. Two fully conjugated covalent organic frameworks as anode materials for lithium ion batteries. J Mater Chem A. 2016;4(37):14106-14110.
- Kang HW, Liu HL, Li CX, et al. Polyanthraquinone-triazine-A promising anode material for high-energy lithium-ion batteries. ACS Appl Mater Interfaces. 2018;10(43):37023-37030.
- 115. Haldar S, Roy K, Kushwaha R, Ogale S, Vaidhyanathan R. Chemical exfoliation as a controlled route to enhance the anodic performance of COF in LIB. Adv Energy Mater. 2019; 9(48):1902428.
- Zhu YZ, Chen XF, Cao YQ, et al. Reversible intercalation and exfoliation of layered covalent triazine frameworks for enhanced lithium ion storage. *Chem Commun.* 2019;55(10): 1434-1437.
- Chen XD, Li YS, Wang L, et al. High-lithium-affinity chemically exfoliated 2D covalent organic frameworks. *Adv Mater*. 2019:31(29):1901640.
- 118. Gu S, Wu SF, Cao LJ, et al. Tunable redox chemistry and stability of radical intermediates in 2D covalent organic frameworks for high performance sodium ion batteries. *J Am Chem Soc.* 2019;141(24):9623-9628.
- 119. Kim MS, Lee WJ, Paek SM, Park JK. Covalent organic nanosheets as effective sodium-ion storage materials. *ACS Appl Mater Interfaces*. 2018;10(38):32102-32111.
- 120. Shehab MK, Weeraratne KS, Huang T, Lao KU, El-Kaderi HM. Exceptional sodium-ion storage by an azacovalent organic framework for high energy and power density sodium-ion batteries. ACS Appl Mater Interfaces. 2021; 13(13):15083-15091.
- 121. Chen XD, Zhang H, Ci CG, Sun WW, Wang Y. Few-layered boronic ester based covalent organic frameworks/carbon nanotube composites for high-performance K-organic batteries. ACS Nano. 2019;13(3):3600-3607.

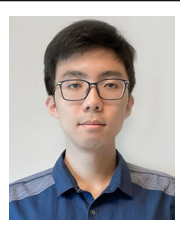
- 122. Zhang QF, Wei HP, Wang LL, et al. Accessible COF-based functional materials for potassium-ion batteries and aluminum batteries. *ACS Appl Mater Interfaces*. 2019;11(47):44352-44359.
- Zhang H, Sun WW, Chen XD, Wang Y. Few-layered fluorinated triazine-based covalent organic nanosheets for highperformance alkali organic batteries. ACS Nano. 2019;13(12): 14252-14261.
- 124. Yin YX, Xin S, Guo YG, Wan LJ. Lithium-sulfur batteries: electrochemistry, materials, and prospects. *Angew Chem Int Ed.* 2013;52(50):13186-13200.
- Liao HP, Ding HM, Li BJ, Ai XP, Wang C. Covalent-organic frameworks: potential host materials for sulfur impregnation in lithium-sulfur batteries. J Mater Chem A. 2014;2(23):8854-8858.
- Liao HP, Wang HM, Ding HM, et al. A 2D porous porphyrinbased covalent organic framework for sulfur storage in lithium sulfur batteries. J Mater Chem A. 2016;4(19):7416-7421.
- 127. Ghazi ZA, Zhu LY, Wang H, et al. Efficient polysulfide chemisorption in covalent organic frameworks for high-performance lithium-sulfur batteries. *Adv Energy Mater.* 2016; 6(24):1601250.
- 128. Xu F, Yang SH, Jiang GS, Ye Q, Wei BQ, Wang HQ. Fluorinated, sulfur-rich, covalent triazine frameworks for enhanced confinement of polysulfides in lithium-sulfur batteries. *ACS Appl Mater Interfaces*. 2017;9(43):37731-37738.
- 129. Meng Y, Lin GQ, Ding HM, Liao HP, Wang C. Impregnation of sulfur into a 2D pyrene-based covalent organic framework for high-rate lithium-sulfur batteries. *J Mater Chem A*. 2018; 6(35):17186-17191.
- 130. Yoo J, Cho SJ, Jung GY, et al. COF-net on CNT-net as a molecularly designed, hierarchical porous chemical trap for polysulfides in lithium-sulfur batteries. *Nano Lett.* 2016;16(5):3292-3300.
- 131. Xu F, Yang SH, Chen X, et al. Energy-storage covalent organic frameworks: improving performance via engineering polysulfide chains on walls. *Chem Sci.* 2019;10(23):6001-6006.
- 132. Vazquez-Molina DA, Mohammad-Pour GS, Lee C, et al. Mechanically shaped two-dimensional covalent organic frameworks reveal crystallographic alignment and fast Li-ion conductivity. *J Am Chem Soc.* 2016;138(31):9767-9770.
- 133. Cai SL, Zhang YB, Pun AB, et al. Tunable electrical conductivity in oriented thin films of tetrathiafulvalene-based covalent organic framework. *Chem Sci.* 2014;5(12):4693-4700.
- 134. Chen HW, Tu HY, Hu CJ, et al. Cationic covalent organic framework nanosheets for fast Li-ion conduction. *J Am Chem Soc.* 2018;140(3):896-899.
- 135. Li Z, Liu ZW, Li ZY, et al. Defective 2D covalent organic frameworks for postfunctionalization. *Adv Funct Mater.* 2020; 30(10):1909267.
- 136. Jeong K, Park S, Jung GY, et al. Solvent-free, single lithium-ion conducting covalent organic frameworks. *J Am Chem Soc.* 2019;141(14):5880-5885.
- 137. Xu Q, Tao SS, Jiang QH, Jiang DL. Ion conduction in polyelectrolyte covalent organic frameworks. *J Am Chem Soc.* 2018;140(24):7429-7432.
- 138. Guo ZB, Zhang YY, Dong Y, et al. Fast ion transport pathway provided by polyethylene glycol confined in covalent organic frameworks. *J Am Chem Soc.* 2019;141(5):1923-1927.
- 139. Bandaru N, Kumar RS, Sneed D, et al. Effect of pressure and temperature on structural stability of MoS2. *J Phys Chem C*. 2014;118(6):3230-3235.

- 140. Zhao YX, Spain IL. X-ray diffraction data for graphite to 20 GPa. *Phys Rev B*. 1989;40(2):993-997.
- 141. Wen YC, Wang XS, Yang Y, et al. Covalent organic framework-regulated ionic transportation for high-performance lithium-ion batteries. *J Mater Chem A*. 2019; 7(46):26540-26548.
- 142. Fang L, Cao XR, Cao ZX. Covalent organic framework with high capacity for the lithium ion battery anode: insight into intercalation of Li from first-principles calculations. *J Phys- Condens Mat.* 2019;31(20):205502.
- Bertolini S, Jacob T. Density functional theory studies on sulfur-polyacrylonitrile as a cathode host material for lithiumsulfur batteries. ACS Omega. 2021;6(14):9700-9708.
- 144. Bahari Y, Mortazavi B, Rajabpour A, Zhuang XY, Rabczuk T. Application of two-dimensional materials as anodes for rechargeable metal-ion batteries: a comprehensive perspective from density functional theory simulations. *Energy Storage Mater.* 2021;35:203-282.
- 145. Xie J, Shi HZ, Shen C, Huan L, He MX, Chen M. Heteroatom-bridged pillar[4]quinone: evolutionary active cathode material for lithium-ion battery using density functional theory. *J Chem Sci.* 2021;133(1):2.
- 146. Hu W, Wang HW, Luo WW, Xu B, Ouyang CY. Formation and thermodynamic stability of oxygen vacancies in typical cathode materials for Li-ion batteries: density functional theory study. Solid State Ion. 2020;347:115257.
- 147. Woo J, Sim ES, Je M, Choi H, Chung YC. Theoretical dopant screening and processing optimization for vanadium disulfide as cathode material for Li-air batteries: a density functional theory study. *Appl Surf Sci.* 2020;508:145276.
- 148. He Q, Yu B, Li ZH, Zhao Y. Density functional theory for battery materials. *Energy Environ Mater.* 2019;2(4):264-279.
- Kim KC, Liu T, Lee S, Jang SS. First-principles density functional theory modeling of redox potential of organic materials for lithium-ion batteries. J Am Chem Soc. 2017;138(7):2374-2382.
- 150. Feng DL, Feng YH, Liu YZ, Zhang WS, Yan YY, Zhang XX. Thermal conductivity of a 2D covalent organic framework and its enhancement using fullerene 3D self-assembly: a molecular dynamics simulation. *J Phys Chem C*. 2020;124(15): 8386-8393.
- 151. Zhang YF, Fang TM, Hou QG, Li Z, Yan YG. Water desalination of a new three-dimensional covalent organic framework: a molecular dynamics simulation study. *Phys Chem Chem Phys.* 2020;22(29):16978-16984.
- Fang QR, Zhuang ZB, Gu S, et al. Designed synthesis of largepore crystalline polyimide covalent organic frameworks. *Nat Commun*. 2014;5(1):4503.
- 153. Huo JQ, Luo BC, Chen Y. Crystalline covalent organic frameworks from triazine nodes as porous adsorbents for dye pollutants. *ACS Omega*. 2019;4(27):22504-22513.
- Ramees PP, Mondal PK, Chopra D. Synthesis and characterization of a 2D covalent organic framework (COF) of hexagonal topology using boronate linkages. J Chem Sci. 2018;130(5):51.
- 155. Liu XL, Li J, Gui B, et al. A crystalline three-dimensional covalent organic framework with flexible building blocks. *J Am Chem Soc.* 2021;143(4):2123-2129.
- 156. Kubisiak P, Eilmes A. Molecular dynamics simulations of ionic liquid based electrolytes for Na-ion batteries: effects of force field. *J Phys Chem B*. 2017;121(42):9957-9968.

- Martin-Garcia F, Papaleo E, Gomez-Puertas P, Boomsma W, Lindorff-Larsen K. Comparing molecular dynamics force fields in the essential subspace. *PLoS One.* 2015;10(3): e0121114.
- 158. van der Jagt R, Vasileiadis A, Veldhuizen H, et al. Synthesis and structure-property relationships of polyimide covalent organic frameworks for carbon dioxide capture and (aqueous) sodium-ion batteries. *Chem Mater.* 2021;33(3):818-833.
- 159. Stephens PJ, Devlin FJ, Chabalowski CF, Frisch MJ. Ab-initio calculation of vibrational absorption and circular-dichroism spectra using density-functional force-fields. *J Phys Chem.* 1994;98(45):11623-11627.
- 160. Ditchfield R, Hehre WJ, Pople JA. Self-consistent molecular-orbital methods 9. Extended Gaussian-type basis for molecular-orbital studies of organic molecules. *J Chem Phys.* 1971;54(2):724-728.
- 161. Marenich AV, Cramer CJ, Truhlar DG. Universal solvation model based on solute electron density and on a continuum model of the solvent defined by the bulk dielectric constant and atomic surface tensions. *J Phys Chem B*. 2009;113(18): 6378-6396.
- 162. Wu MM, Zhao Y, Sun BQ, et al. A 2D covalent organic framework as a high-performance cathode material for lithium-ion batteries. *Nano Energy*. 2020;70:104498.
- 163. Singh V, Kim J, Kang B, et al. Thiazole-linked covalent organic framework promoting fast two-electron transfer for lithium-organic batteries. Adv Energy Mater. 2021;11(17): 2003735.
- 164. Song XD, Zhang MR, Yao M, Hao C, Qiu JS. New insights into the anchoring mechanism of polysulfides inside nanoporous covalent organic frameworks for lithium-sulfur batteries. ACS Appl Mater Interfaces. 2018;10(50):43896-43903.
- Klimes J, Bowler DR, Michaelides A. Chemical accuracy for the van der Waals density functional. *J Phys Condens Matter*. 2010;22(2):022201.
- 166. Wang ZQ, Gu S, Cao LJ, et al. Redox of dual-radical intermediates in a methylene-linked covalent triazine framework for high-performance lithium-ion batteries. ACS Appl Mater Interfaces. 2021;13(1):514-521.
- 167. Zhu P, Meunier V. Electronic properties of two-dimensional covalent organic frameworks. *J Chem Phys.* 2012;137(24): 244703.
- Sinha N, Pakhira S. Tunability of the electronic properties of covalent organic frameworks. ACS Appl Electron Mater. 2021; 3(2):720-732.
- Pakhira S, Lucht KP, Mendoza-Cortes JL. Iron intercalation in covalent-organic frameworks: a promising approach for semiconductors. J Phys Chem C. 2017;121(39):21160-21170.
- 170. Pakhira S, Mendoza-Cortes JL. Intercalation of first row transition metals inside covalent-organic frameworks (COFs): a strategy to fine tune the electronic properties of porous crystalline materials. *Phys Chem Chem Phys.* 2019;21(17):8785-8796.
- 171. Kang ZX, Peng YW, Qian YH, et al. Mixed matrix membranes (MMMs) comprising exfoliated 2D covalent organic frameworks (COFs) for efficient CO<sub>2</sub> separation. *Chem Mater*. 2016; 28(5):1277-1285.
- 172. Paier J, Hirschl R, Marsman M, Kresse G. The Perdew-Burke-Ernzerhof exchange-correlation functional applied to the G2-1

- test set using a plane-wave basis set. *J Chem Phys.* 2005; 122(23):234102.
- 173. Grimme S, Antony J, Ehrlich S, Krieg H. A consistent and accurate ab initio parametrization of density functional dispersion correction (DFT-D) for the 94 elements H-Pu. *J Chem Phys.* 2010;132(15):154104.
- 174. Eremin RA, Zolotarev PN, Ivanshina OY, Bobrikov IA. Li(Ni, Co,Al)O-2 cathode delithiation: a combination of topological analysis, density functional theory, neutron diffraction, and machine learning techniques. *J Phys Chem C*. 2017;121(51): 28293-28305.
- 175. Okamoto Y, Kubo Y. Ab initio calculations of the redox potentials of additives for lithium-ion batteries and their prediction through machine learning. *ACS Omega*. 2018; 3(7):7868-7874.
- 176. Allam O, Kuramshin R, Stoichev Z, Cho BW, Lee SW, Jang SS. Molecular structure-redox potential relationship for organic electrode materials: density functional theory-machine learning approach. *Mater Today Energy*. 2020;17:100482.
- 177. Allam O, Cho BW, Kim KC, Jang SS. Application of DFT-based machine learning for developing molecular electrode materials in Li-ion batteries. *RSC Adv.* 2018;8(69):39414-39420.
- 178. Li W, Xia XX, Li S. Screening of covalent-organic frameworks for adsorption heat pumps. *ACS Appl Mater Interfaces*. 2020; 12(2):3265-3273.
- 179. Ongari D, Yakutovich AV, Talirz L, Smit B. Building a consistent and reproducible database for adsorption evaluation in covalent-organic frameworks. *ACS Cent Sci.* 2019;5(10):1663-1675.

#### **AUTHOR BIOGRAPHIES**



Shikai Jin is currently a PhD student under the supervision of Prof. Seung Woo Lee at Georgia Institute of Technology. He received his BS and MS degree in Mechanical Engineering from the Georgia Institute of Technology in 2018 and 2020, respectively.

His current research interests focus on organic electrode nanostructures for electrochemical energy storage and conversion systems.



Omar Allam is a Graduate Research Assistant at the Georgia Institute of Technology. Omar received his BS and MS in Mechanical Engineering from the Georgia Institute of Technology in 2018 and 2020, respectively. His current research interests include

using computational methods such as density functional theory, molecular dynamics, and machine learning approaches to investigate a wide range of organic and hybrid organic–inorganic materials for optoelectronics, and energy storage and conversion applications.



**Seung Woo Lee** is an Associate Professor of Mechanical Engineering at Georgia Institute of Technology. He received his BS in Chemical Engineering from Seoul National University with Summa cum laude (2004) and PhD in Chemical Engineering

from Massachusetts Institute of Technology (2010). His research has been focused on nanostructured electrodes for electrochemical energy storage and conversion systems. He is the recipient of the National Science Foundation CAREER Award, the National

Aeronautics and Space Administration Early Career Faculty Award, the Hanwha Advanced Materials Non-Tenure Faculty Award, and the Korean-American Scientists and Engineers Association (KSEA) Young Investigator Grant Award.

**How to cite this article:** Jin S, Allam O, Jang SS, Lee SW. Covalent organic frameworks: Design and applications in electrochemical energy storage devices. *InfoMat.* 2022;1-35. doi:10.1002/inf2.12277